

Reply to reviewers - Drivers of Pine Island Glacier speed-up between 1996 and 2016.

Jan De Rydt, Ronja Reese, Fernando S. Paolo, G. Hilmar Gudmundsson

October 7, 2020

1 Reply to Anonymous Referee 1

This is a nice paper showing some well-constructed model experiments designed to understand the sensitivity of PIG to various parameter. Despite my many comments and criticisms, I would very much like to see this paper published and I think it makes a valuable contribution to the field.

We thank the reviewer for their kind support.

I would like to see more discussion on the quality of the data and how it affects the results. To me the quality of the 1996 data from radar altimetry are highly suspect – ERS DEMs can be off by 10s or 100s of meters in places. Figure 1c does nothing to improve my confidence in these data, particularly the strong gradient in the thickness change across the ice shelf, with nearly zero thinning on the shelf centerline. Thus, I expect some model discrepancies could be explained by errors in the data sets used to constrain the model.

As the reviewer correctly points out, satellite altimeters have limited accuracy, which means they are less reliable for DEMs. However, they are very precise instruments, which makes them excellent for change detection. That is why we did not use a snapshot DEM for the 1996 geometry (such as those based on ERS data), but compiled a time series of height changes from an extensive set of overlapping satellite altimeter data, as described in App.A. To derive net thickness changes between 1996 and 2016, we have integrated the altimeter trend over a 20-year time interval, which is very robust. To obtain ice thickness for 1996, altimeter thickness changes were subtracted from the Bedmachine reference thickness, based on REMA. The REMA DEM has very high resolution (good in the horizontal component), but has no way to constrain the vertical component of floating ice, as it is derived from optical sensors. So the surface elevation derived from REMA, like Bedmachine used here, is in fact tied to CryoSat-2. Appendix A in the main paper discusses a number of limitations of this approach, including uncertainties within a buffer along the grounding line. To gain additional confidence in our 1996 ice thickness distribution, we compared the grounding line location in the model to independent data from DInSAR (Rignot et al., 2014). We have added a new Figure to Appendix A (see Figure 1 below) to show that they agree well. The reviewer also highlights the ‘nearly zero thinning on the ice shelf centerline’. The near-zero or positive thickness changes in this area are consistent with previously observed and published data, and we refer to e.g. Joughin et al. (2019) (their Figure 2 and supplementary data) and (Lhermitte et al., 2020) for more details.

Related to this issue, I would rather see results like Figure 4b expressed as changes in basal shear stress. Particularly in light of the noisy 1996 data set, I would expect inferred changes in basal shear stress to be largely due to topographic (driving stress) errors.

We hope that our discussion above has taken away the reviewer’s concerns about the quality of the 1996 ice thickness data. With regards to Figure 4b, we present the corresponding changes in basal shear stress τ_b in Figure 2 below. The changes are largest in the vicinity of the grounding line, as expected, and there is no obvious correlation to noise in the topography. In particular, changes in driving stress along the central fast-flowing trunk are small, and most of the increased forward motion of the glacier (U_b in Eq. 4 of the manuscript) is captured by changes in C , as shown in Figure 4b of the manuscript.

As mentioned in some of the comments below, I have concerns about the joint inversion comment for A and C. While some prior info seems to be used, it’s not well documented in the appendix. For

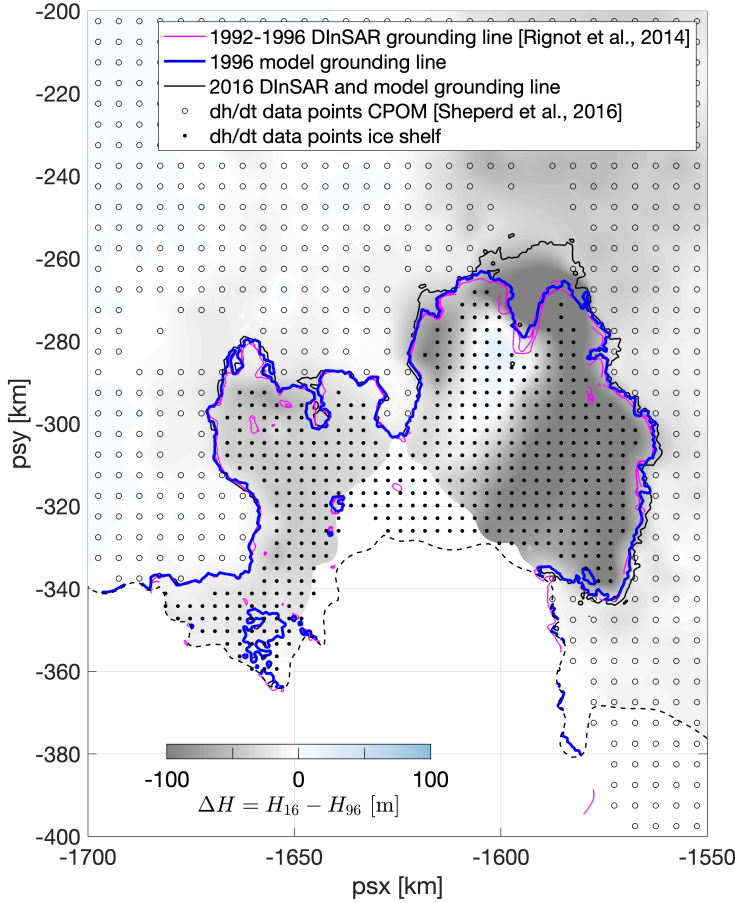


Figure 1: New figure added to Appendix A showing model and DInSAR grounding lines, altimeter data coverage for $\frac{dh}{dt}$ between 1996 and 2016 (dots and circles), and the total $\Delta H = H_{16} - H_{96} = \int_{96}^{16} \frac{dh}{dt} dt$ field used in this study (grey to blue background color).

example, do the p priors allow greater variation of A in the margins, while suppressing it elsewhere. I suspect not from the outputs. The inversions for A bear no resemblance to what my intuition would say the distribution should look like. There are numerous papers debating factors of 10 enhancement in shear margins, but this solution as irregular, patchy variations that vary by more than a factor of 100 (shouldn't the priors have not let A vary so much), sometimes with blobs of effectively very cold/stiff ice crossing the margins. I would really have liked the results better if the inversions for A had been restricted to the shelf where they don't make an already ill-posed problem even more so. This would have allowed for better discrimination of any role damage (A enhancement) on the ice shelf shear margins.

We extended the accompanying text for the cost functions (Eq. B1 and B2) in the Appendix. In particular, we now stress that the regularization terms contain a gradient and an amplitude contribution, both of which are multiplied by a spatially constant prefactor. The role of the gradient premultiplier, γ_s , was discussed at length in Appendix D. However we did not elaborate on the dependency of our results on the amplitude premultiplier, henceforth called γ_a . The value of γ_a was set to 1 throughout our simulations, but it is in fact a model parameter, which controls the weights of the C and A amplitude terms in the cost function. For example, $(g_a)_A \gg 1$ would force the final solution for A to be 'close' to the prior, hence suppressing any large spatial variations in A . To use a spatially varying g_a to allow greater variations of A in some areas (such as the shear margins) based purely on heuristic arguments, seems rather ad-hoc. We therefore keep g_a constant throughout the domain. An L-curve analysis, similar to Figure A1b for γ_s , was used to determine the optimal choice $\gamma_a = 1$. As the reviewer points out, some modeling groups do indeed set $A = A_{\text{prior}}$ for the grounded ice. In our view this does not make the ill-posed problem better behaved. Instead,

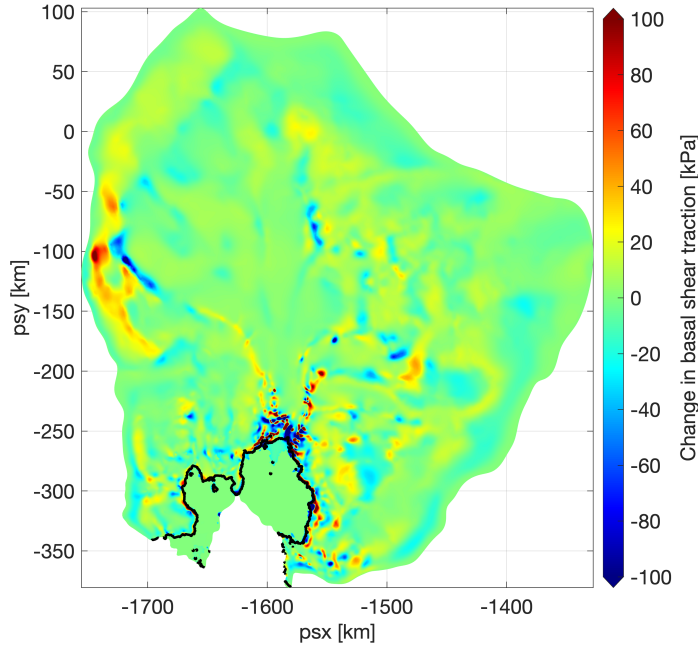


Figure 2: Changes in basal traction for the \mathcal{E}_C^3 experiment.

it assumes that one has perfect knowledge about A for the grounded ice (i.e. $A = A_{\text{prior}}$ exactly, everywhere). This is a strong assumption that might be far from the truth, as significant uncertainties in (depth-integrated) ice temperature, damage and fabric persist for the grounded ice, all of which should be captured by spatial variations in A . Given the range of physical properties that potentially influence A , it seems incorrect to interpret the latter in terms of temperature/damage alone, and the spatial distribution might therefore not always be intuitive. Nevertheless, the highest values of A in Figure A1 are primarily constrained to the shear margins, which is consistent with our expectations. To comprehensively address the ambiguities associated with different inversion methods and model parameters requires a full Bayesian treatment, which, we feel, is beyond the scope of this study.

Other papers have presented similar results using a forward approach with somewhat better agreement with the data, though for a shorter time period (e.g., Gillet-Chaulet et al 2016 and Joughin et al 2019). There is some discussion about this work, but more comparisons could be drawn. For example, to get good agreement by assuming a reduction in basal traction near the grounding line driving by height-above flotation (effective pressure) variations. Could something like that be done here.

We agree that Coulomb-limited sliding laws can have an important impact on the model response to changes in geometry, in particular in the vicinity of the grounding line, as demonstrated by e.g. Gillet-Chaulet et al. (2016) and Joughin et al. (2019). Although the analysis in this study has expanded the often-used Weertman law with $m = 3$ exponent to allow for a spatially heterogeneous exponent, we were unable to fully reproduce observed flow changes in the vicinity of the grounding line. Coulomb-limited sliding might lead to an improved fit, and although such experiments should be carried out as part of a separate study, we have expanded our discussion on this topic in Section 3.3.

The colour maps are all in shades of red are hard to interpret. Maybe a different colour map or contours would help.

We have tried to make our figures colorblind friendly and have experimented with various alternative colormaps, but did not find these to be particularly helpful. We have added a 50% contour to figures 3 and 5 to better guide the readers' eye.

Line 27: Would be fair to cite Seroussi et al 2014 (doi:10.5194/tc-8-1699-2014) and Joughin et al, 2010 (in refs) in this list. Alternatively, these might be better in line 34.

Thank you for suggesting these references; we have added both.

Line 70-75. Where does loss of traction due grounding line fit it, which is caused by thinning (this is probably a bigger factor than the original loss of buttressing that triggered it – e.g., Figure 4 Joughin 2019 ref, which thinning alone can actually slow ice shelf a GL velocities without the loss of traction from ungrounding). Payne et al 2004 also look at the shift of the GL, rather than just the loss of ice shelf thinning.

The loss of basal traction due to ungrounding is represented in experiments $\mathcal{E}_{\text{Thin}}^m$, which prescribes observed thickness changes of both the floating and grounded parts including any associated grounding line movement. We have clarified this point in the manuscript.

Line 84 $\Delta U_A + \Delta U_C = 0$. Again is the loss of traction as the grounding line retreats being bookkept as a change in ΔU_C or a change ΔU_{thin} . This is also important for interpreting line 95 because the paper cited shows the thinning driven response, but that includes loss of traction as the ice approaches flotation and finally ungrounds. All I am asking here for is a sentence clearly stating where the loss of traction due to ungrounding is bookkept.

Thank you for asking us to clarify this important point. The loss of traction due to grounding line (GL) retreat is simulated in $\mathcal{E}_{\text{Thin}}^m$, which accounts for all observed thickness changes between 1996 and 2016 and therefore includes GL movement. We have added a sentence to emphasise this point. The modelled changes in GL position correspond almost exactly to observed changes from DInSAR, yet, changes in geometry (incl. loss of traction) were not generally sufficient to explain the speed-up of PIG between 1996 and 2016. At least not in our model setup with Weertman sliding exponent $m = 3$. To account for any remaining discrepancies between modeled and observed surface velocity in 2016, two possibilities were explored: experiment \mathcal{E}_C^3 was set up to determine what additional changes in the slipperiness would be required to account for the remaining changes in speed, whereas \mathcal{E}_A^3 was set up to determine changes in the rate factor required to account for the remaining changes in speed.

Line 139. “The resulting values for ΔH , linearly interpolated across the grounding line and in data sparse areas, are shown in Fig. 1c” I don’t see how this is valid or maybe I am not understanding what is being done. You could have a case where the shelf thins by 10s or 100s of meters due to melting, but the grounded change in thickness is far less. Am I misinterpreting something.

The data coverage used to derive thickness changes between 1996 and 2016 is shown in the new Figure A1 (see Fig.1 above). Within a 3 km buffer downstream of the grounding line we did not have any reliable altimetry measurements, and linear interpolation of ΔH across this buffer could indeed lead to an underestimate of ice shelf thinning. For the remainder of the domain, data sparse areas largely correspond to recently ungrounded parts of the central glacier. If one assumes near-constant thinning of the ice shelf and a steady retreat of the grounding line in this area, linear interpolation of thickness changes seem appropriate. As an independent check, the resulting changes in grounding line position closely follow the DInSAR measurements.

Line 165. “linear, viscous or close-to plastic” It should be “linear viscous, non-linear viscous, or close to plastic”

Thank you for spotting this incorrect use of terminology.

Line 167: “which caused small variations in τ_b between cases,“ This has to do with the interplay between A and τ_b , not so much the exponent. If you had used a fixed A, then τ_b is in fact what you are using to achieve stress balance with its parameterization via the sliding law (any sliding law). So, I am not sure the following sentence is correct and probably should be removed. What is different about the two studies is that A is determined on the entire domain for this study vs only on the shelf. A such additional degrees of freedom are introduced, which will give a better fit to the data, but could result in model parameters that are far from the true physical values (eg. To stiff A balanced by a too slippery bed). Given that the response is dependent on the flow and sliding law parameters, the accuracy of the fit is somewhat immaterial. There is a counter argument that many other studies fit for one parameter or another using an assumed value for the other, so there could be errors in the assumed value. But I am not seeing a strong case for the improvement here.

We have removed the sentence “We consider our approach to be more appropriate for this study, as our focus is primarily on an accurate model representation of the surface flow (e.g. Eq. 2).”

which also confused reviewer 2. We agree that both methods (i.e. separate inversions for different values of m vs. a single inversion for $m = 1$) are both valid and differences are irrelevant for our results.

Line 172: I may be playing with semantics here but what is obtain is not a “best estimate” it’s an estimate that produces the best fit, but as mentioned above, this by no means ensures that it is the best estimate.

This is a very valid point. In fact, using ‘an estimate that produces the best fit’ is also debatable, as the inversion is more than just a fitting exercise. To be precise our statement should be phrased in the context of the cost function, which contains prior information and error estimates. In the interest of clarity we have decided to remove this sentence.

Line 176 “basal slipperiness were kept fixed” Please how the ungrounded region is treated – either here or above. While it may seem obvious, when various parameters are being held fixed, it’s not always immediately clear that the traction is being zeroed when the ice goes afloat.

We will add a sentence here to explain that areas where changes in ice thickness cause ungrounding of the ice, this automatically implies that $\tau_b = 0$ and the value of C becomes irrelevant. For areas that remain grounded, C is kept fixed.

Line 451: Why not initialize with an A estimated from temperature model; solutions are often better if you start nearer the answer. Also given that there are blobs of A in close proximity each other that can vary by a couple of orders of magnitude (a difference between ice at 0 and -30 deg) without any real correspondence to the flow pattern (outside of some shear margins) it would be worth some comment here about how physically realistic the solution is at least in a qualitative sense. Even for shear margins, the lower trunk on the west side where you would expect some enhancement, the ice actually looks like it’s much stiffer than the reference -15 deg.

Besides the sensitivity experiments presented in Appendix D, additional experiments were performed to test the robustness of the inversion results, in particular the A field. We did not include these results in the manuscript, but are happy to provide more details here. The first set of experiments, as outlined in one of our replies above, aims to test the sensitivity of A to the value of $(g_a)_A$ in the cost function. The pre-multiplier $(g_a)_A$ effectively controls how ‘far’ the solution A is allowed to deviate from its prior value A_{prior} . Results are summarized in Fig.3 (first row) and can be emphasised as follows: For $(g_a)_A \leq 1$, the solution for A and corresponding misfit (I , Eq.B1 in the main text) do not vary much. For $(g_a)_A \gg 1$, A is forced to be close to the prior value, as expected, and the misfit I increases. In the latter case, variability in the flow does not automatically get absorbed into larger variability of the slipperiness, C , and reducing $(g_a)_C$ does not change this conclusion. An L-curve approach was used to determine the optimal values $(g_a)_A = 1$ and $(g_a)_C = 1$ for our experiments. We are not aware of reliable depth-average ice temperature estimates that can be used as prior values in this region, and even if they existed, spatial variations of other ice properties (damage, fabric,...) upstream of the grounding line would still need to be inverted for. To partly address this issue, we assessed the sensitivity of A to the prior value in a the second set of experiments. Separate inversions were performed for $A_{\text{prior}} = -5C, -15C$ (the default) and $-25C$. Results (bottom row of Fig. 3) show that A_{prior} does not have a significant effect (both qualitative and quantitative) on the final A field for ice that is not close-to-stagnant, and the spatial distribution of A is robust. Finally, we would like to mention that we have been pursuing some of these points in recent work on Thwaites Glacier. We kindly refer the reviewer to Barnes et al. (2020), currently in discussion, for a detailed analysis of inversion products for different models (ISSM, \dot{U}_a and STREAMICE). some of these indeed use temperature estimates as part of the prior and/or assume perfect knowledge about A for grounded ice.

Line 216: Would be nice to have a brief introduction to this section between 3 and 3.1. Actually this would be a good place to describe the flux gates, which break up the flow of the text below.

Line 232-237.5: Please consider moving this flux gate description to intro paragraph before 3.1 as described above.

We thank the reviewer for this suggestion, and have moved our description of the flux gates to the start of Section 3.

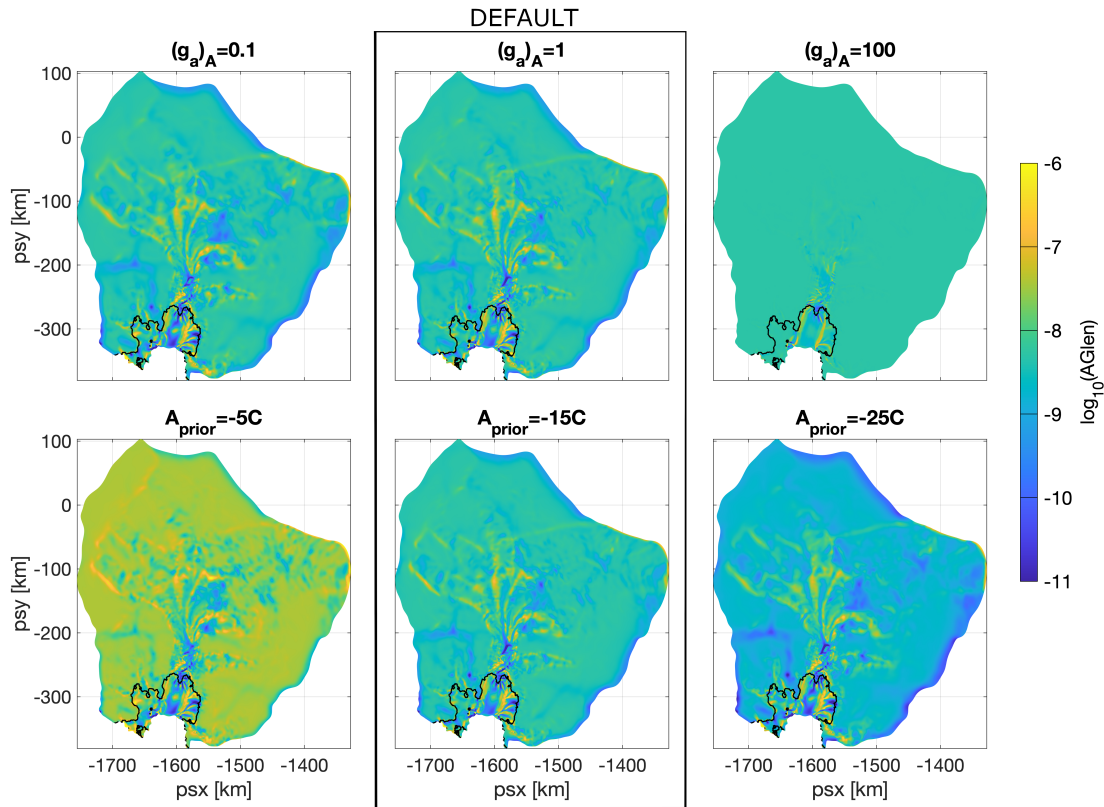


Figure 3: Sensitivity of A to variations in key inversion parameters.

Line 221: “viscous, rate-strengthening bed rheology “ Please add “non-linear” viscous here. Also please note that this description applies under the assumption of till at the ice bed interface. As conceived, the original Weertman law applies to sliding over a hard, non-deforming bed, with ice and rock separated by a thin water film. Inversions here and elsewhere suggest both types of bed may be present beneath PIG. To the extent that its applicable to till, its likely only at low sliding speeds (see Zoet reference).

We acknowledge the reviewer’s earlier comment to use “linear viscous, non-linear viscous, or close to plastic” for the different types of rheology, and for stressing that a non-linear powerlaw describes both hard-bedded sliding (as originally conceived by Weertman), and till deformation, as outlined by Zoet and Iverson (2020).

Line 224-225: 50% speedup. Be clear on where, it looks like this magnitude really applies only to the outer shelf. Might also be good to note that results are consistent with the Schmeltz et al 2002 reference that is cited in the text, where a similar experiment was performed (they only get a speedup of 40% right at the shelf front – mid shelf its more like 20%). Would be far more accurate to say “restricted to the OUTER ice shelf”. A lack of speed from calving at the GL is consistent with a number of published results showing speed on PIG over the last decade, during which time there have been large calving events.

We will add “OUTER shelf” to better pinpoint the geographical extent of instantaneous speed-up induced by calving, and refer to Schmeltz et al. (2002) to emphasize consistency with earlier studies.

Line 237: “This supports...” This what? How about something like “This moderate response supports...” Now please cite the earlier works that your work supports.

We have moved the preceding sentences about the flux gates to the start of the section, and have blended the last two sentences of this paragraph to say “Figure 3e shows that the retreat of the PIG calving front between 1996 and 2016 accounts for 2% and 13% of the observed flux changes through

Gate 1 and 2 respectively, which indicates minor instantaneous changes to the flow upstream of the grounding line.”

Lines 239-243: This text could be wordsmithed – there are at least 3 places saying something about the similarity to calving response. Could just say something like “The responses to calving and thinning are similar at the flux gates, but the calving induces a larger response on the outer shelf (50% vs \downarrow 25%). “Ice shelf thinning is generally accepted to be the main driver of ongoing mass loss of PIG, and patterns of ice shelf thinning elsewhere in Antarctica are strongly correlated to observed changes in grounding line flux (Reese et al., 2018; Gudmundsson et al., 2019).” This is a gross over-simplification of the conventional wisdom, which is that loss of buttressing can induce near GL thinning, which leads to retreat, which induces more loss. As AR5 notes, “Problems arise at the GL because, in addition to flotation, basal traction is dramatically reduced as the ice loses contact with the underlying bedrock (Pattyn et al., 2006). This is a topic of active research, and a combination of more complete modelling of the GL stress regime (Favier et al., 2012) and the use of high-resolution (subkilometre) models (Durand et al., 2009; Cornford et al., 2013) shows promise towards resolving these problems.” Numerous studies have shown that the near GL speedup is a response to the loss of traction as the GL retreats, not the thinning itself, although that thinning is believed to have triggered the whole process, likely through smaller speedups that thin the GL to flotation.

We of course agree with the reviewer, and we are aware of the GL processes that cause glacier speed-up (this is the subject of our study). We do not believe that our statements are a “gross over-simplification”. In particular, our sentence “the force perturbations that result from ice-shelf thinning alone, in particular the instantaneous reduction in back forces τ_{IS} , are not sufficient to explain the magnitude of observed changes in upstream flow” echoes the reviewer’s comments. We go on to explain that “time-evolving changes in geometry and mass redistribution upstream of the grounding line play a significant role in increasing the dynamic response of the glacier”. In a revised version of the manuscript, we will add that the dynamic response includes grounding line movement and associated changes in basal traction.

Line 246: “in upstream flow, CONSISTENT WITH OTHER STUDIES THAT HAVE SHOWN SIMILAR RESULTS [e.g., Payne 2004, Joughin 2010, 2019, Seroussi, 2014, Schoof 2007....].

Done.

Line 271 please add also “non-linear” before viscous. Also “non linear viscous bed rheology described by a Weertman sliding law”. Weertman is not a viscous flow model even if the expressions are mathematically equivalent and generally is taken to mean an exponent between 2 and 3. Since your law applies to a broader range of exponents and indeterminate bed conditions (probably both till and hard bed), how about just substituting here and above power-law sliding in place of Weertman sliding law. At some point where you used $m=3$ you can say “power-law sliding with $m=3$, which for hard beds corresponds to a Weertman sliding law” to credit Weertman (a reference to his work would be nice).

Thank you for clarifying these nuances in terminology. So far we have consistently used ‘Weertman law’ to refer to any sliding law that takes the form in Eq.4, irrespective of the exponent value. We have no objections against using ‘Weertman law’ for $m = 3$ only, and ‘powerlaw’ for $m \neq 3$. We will adjust the text accordingly.

Line 290 “Weertman sliding” change to “power law sliding”.

Done.

Line 300: Change “Weakening of the ice in these areas accounts for” to “Weakening of the ice in these areas is sufficient to account for”... Its only one model on the knob, so it’s a sufficient but not necessary condition.

Good point, thank you. We will change this sentence as suggested.

Line 302-303: I agree this change is physically improbable. But as noted above, so is the original A, which effectively has very warm ice in the margin just upstream of the margin where the ice is very cold. See other comments about this.

Thank you. We hope to have addressed the other comments in our earlier replies.

Line 368: The result is also consistent with the Schoof type sliding law used by Joughin et 2019, which produces Coulomb plastic like behavior at speeds ≥ 300 m/yr and low- m (Weertman-like) behavior at slower speeds. The areas with plastic like behavior in Figure 6 transition to lower exponents in the area between the 600 and 100 m/yr contours shown in Fig 4, which would be worth commenting on.

Thank you for pointing this out. We will draw further attention to the analogies between our work and (Joughin et al., 2009).

Line 387: “Compared to spatially uniform values of m ...”. But this in effect what a sliding law like that proposed by Schoof (and in another paper by Gagliardini et al) does – provides high- m behavior for fast flow and low- m behavior for slow flow.

We agree. Our analysis has provided a way to bracket plausible values and a spatial distribution of m .

Line 399: Change “Based on the most comprehensive observations...” By what metric? Other data sets are arguably more comprehensive (you have only 2 snapshots in time). Whether they are or are not the most comprehensive has no bearing on the value of this paper. Instead, simply say “Based on a comprehensive...” and you are on firm ground.

We again apologize for the misunderstanding about our 1996 geometry. This is indeed a ‘snapshot’ geometry, i.e. with a fixed timestamp, but not based on ‘snapshot’ (ERS1-2) measurements. Instead, the 1996 DEM is based on a comprehensive timeseries of altimeter thickness changes, subtracted from the 2016 REMA DEM, referenced wrt Cryosat-2 data. Further details are provided in one of our earlier replies and Appendix A.

Line 402: Remove “unprecedented”. There are some nice results in this paper, but they largely echo the results of earlier work (I mean no slight here this is true of most papers).

Done.

Line 408: See general comments, but Joughin et al for a different time period got quite close agreement in a similar set of experiments by changes in basal shear stress proportional to the height above flotation in the region immediately above the grounding line. A compare and contrast sentence on this point would be good.

We agree, and will add a sentence at the end of Section 3 to re-iterate this point.

L410: we found that the recent increase in flow speed of Pine Island Glacier is only compatible with observed patterns of thinning if a heterogeneous, predominantly plastic bed underlies large parts of the central glacier and its upstream tributaries, CONSISTENT WITH EARLIER FINDING (there are several that are appropriate).

We will add the suggested text here. References to stress consistency with earlier findings have been added at appropriate places in the manuscript, partly in response to the reviewer’s comments, and we don’t see any point in repeating this long list of references in the conclusions.

2 Reply to referee 2 Stephen Cornford

This paper attributes the speed up in Pine Island Glacier over a 20 year period to a combination of ice thinning, calving front change and rheological change. It concludes (as have others) that the PIG trunk appears to be subject to Coulomb sliding, at least in some parts. This is a well written paper based on sound methods. I do have some minor issues with the manuscript.

We thank the reviewer for their kind support.

L65 (eqn 2). The right hand side does not make sense to me for the reasons you point out later: you can’t determine these things individually and then add them up. You can certainly (as you do) look at each in turn, and even talk about combinations. I can see why you want a notation like this, but at the end of the day, the equation is not correct given the usual definition of addition.

We originally added this equation to help us introduce the notations $\Delta U_{\text{Calv}}, \dots$, but in hindsight we agree that this is incorrect and confusing. We have deferred the definitions of ΔU_{Calv} , etc. to Section 2, where it becomes clear within the model context what these changes in velocity are.

L165 : The inverse problem is solved for each m, and Tb is slightly different. But that would not be so if the velocity were the same in each case, and the velocity could be the same in each case (in the optimal case, equal to the observations). The differences must be due to optimization method or similar. Joughin’s method is equally valid, so you should not claim that yours is more appropriate.

A similar point was raised by reviewer#1. We fully agree and have removed this statement from the ms.

L30: “model studies have primarily focused on the important problem of simulating the response of PIG to a potential anthropogenic intensification of melt.” Perhaps – but Joughin 2010 and 2019 were also concerned with attributing cause to observed change. This is mentioned later (from L42), so you have not neglected these papers, but it does make it makes ‘primarily’ incorrect

Good point, and we will change the sentence: “...several model studies have focused on...”

L95: Joughin et al. (2019) and Joughin 2010

Reference added.

2.2.1 Inverse experiments, and general use of inverse in a ‘slang’ fashion. These are optimization experiments, which involve solution of inverse problems. Ua does not have inverse capability, it has optimization capability.

Agreed. We have changed the title of the subsection and replaced ‘inverse’ with ‘optimization’ elsewhere for consistency.

Figure 3. Either have ‘unaccounted’ bars in every row, or none.

Bars have been removed.

L362. $m_{\text{optimal}} = f_2/(f_1-1) ? 100\% \neq 100$.

Indeed, we want $\Delta U_{\text{CalvThin}}/\Delta U = 1$ and therefore $m_{\text{optimal}} = f_2/(f_1 - 1)$. Thank you.

L500 “In a Bayesian framework, the regularization plays the role of a prior and is added to the misfit, which corresponds to the likelihood”. Tikhonov regularization can be seen as derived from Bayes rule with certain assumptions about the priors. But the methods used here are, I would say, not derived from Bayes rule because the prior is not determined from additional observation or theory: it is chosen to regularize the solution, and the relation to Bayes rule is incidental. Maybe a personal bugbear of mine.

Thanks for pointing out this potential confusion. Since we do not employ the Bayesian framework, we have removed the comment.

3 Reply to Anonymous Referee 3

The manuscript “Drivers of Pine Island Glacier retreat from 1996 to 2016” by J. De Rydt and colleagues analyses the role of several processes in causing the observed changes of Pine Island Glacier between 1996 and 2016 using numerical modeling. They estimate the relative role of calving, ice shelf thinning, ice shelf and ice sheet thinning, and well as combinations of these changes and their ability to reproduce the observed changes in ice velocity. The manuscript is well written, well explained, the figures are appropriate and this work is important as we try to better understand the glacier’s changes in this region.

We thank the reviewer for their kind support.

There is one major point, however, that I would like to see addressed to make sure the results are robust and the conclusions not impacted by model parameter. The 1996 velocities are reproduced by inverting simultaneously the rigidity parameter A and the basal friction parameter C. This has been done in several studies, however there is an infinite combination of these two parameters that can yield similar velocity fields with drastically different values for each of the parameters. This

is something that is observed for the inversion of 2016 in the present manuscript: two additional inversions are done to fit the velocity observations for that year, one changing only C, and the other one changing only A. Therefore, two different combinations of parameters (A1996 with C2016 and A2016 with C1996) yield similar velocity fields in agreement with the 2016 observations. This is a recurrent problem in our field and the alternatives are limited, however I am wondering if a different combination of parameters would lead to different conclusions and I would like to see this point addressed. One solution to do so could be for the 1996 observations to first optimize the friction parameter and then the rigidity parameter in a first case, while a second case would first optimize the rigidity parameter and the friction afterwards. I expect these two cases to exhibit significant differences as most of the misfit will be captured by the first model parameter inferred, with the second one only capturing “residual-like” misfit. Experiments done with these two initial conditions will allow to make sure that the conclusions are robust and not impacted by the choice of these parameters. As explained in detail above, I would like to make sure that the conclusions are robust under a range of values for A and C as both parameters are unconstrained. Additional experiments with other values such as proposed above would help ensure that this is the case.

We agree that the problem is ill-posed, and the solution is -to some degree- dependent on the optimization scheme, which is different for all models. Inverting first for A and then for C, or vice versa, as the reviewer suggests, has potential pitfalls. As the reviewer mentions, it pushes most of the explanation of observed velocities into one of the variables with the other variable only explaining misfits produced by this procedure in the first step. There is no physical basis to think that one variable A or C is of higher order importance in explaining observed velocities. Instead, we have experimented with different regularization parameters, as detailed in further replies below, to make sure that our results are robust. In particular, we have changed the relative weights of amplitude and gradient terms in the cost function, to force closer/looser agreement with prior values, and/or allow greater/smaller spatial variability. In the end, optimal values for the weights were obtained using an L-curve approach, as detailed in a later reply and App.B in the manuscript.

The role of grounding line retreat is confusing. It is not part of ice shelf thinning, but it is included in the ice sheet plus ice shelf thinning. Would it be possible to separate it more from the other processes? The grounding line retreated significantly between 1996 and 2016 for this glacier and it would therefore be interesting to know how much the grounding line evolution contributed to the acceleration. The text about grounding line is also not always clear: it is not included as a separate process, but it is sometimes mentioned along other processes (e.g not mentioned in the abstract, previous studied about grounding line retreat only mentioned in the introduction, stated separately from the rest in conclusions, etc), so I would like to see addressed in a similar way throughout the manuscript. Part of this confusion might come from the problem that grounding line retreat is not clearly separated from other processes.

*Many thanks for raising this point of confusion. We changed the title to “Drivers of Pine Island Glacier **speed-up** between 1996 and 2016” to be clear about the actual aim of the study. Specifically, we prescribe observed changes in the geometry (ice thickness changes and calving) and diagnose the resulting velocity changes in the model. Grounding line retreat and associated loss of basal traction is therefore part of the $\mathcal{E}_{\text{Thin}}$ experiments. The effect of grounding line movement cannot be disentangled from changes in grounded ice thickness, as the grounding line moves due to changes in ice thickness at and upstream of the grounding line over time. However, the effect of reduction in basal traction in newly ungrounded regions could be disentangled from the effect of grounded thickness changes. This could be assessed by targeted new experiments, as the reviewer suggests, looking into the effect of basal traction reduction (i.e. zeroing basal traction where ice ungrounds) without changing the geometry. Such an experiment, albeit well-defined, will not change the main conclusions of our work, namely that the model is unable to reproduce observed changes in speed in response to ice thinning, GL retreat and calving (at least for $m = 3$). We already present a comprehensive set of experiments, which include the loss of basal traction as part of $\mathcal{E}_{\text{Thin}}$, and therefore prefer to keep the suggested experiments as part of a future study.*

These experiments investigate the instantaneous response to changes in geometry. In some places of the text, it is clearly stated, but in other places it is not clearly stated.

Our approach is indeed different from a full transient simulation, whereby the model simulates both changes in ice geometry and velocity. Our experiments could be seen as a ‘hybrid’, whereby changes

in ice geometry are prescribed, but the model diagnoses changes in flow. As we can directly compare modelled and observed changes in flow, our experiments provide a well-constrained framework to validate the model response function, defined by the model physics (SSA, powerlaw sliding, Glen's rheology etc). We note that diagnostic experiments are justified by the instantaneity of the Stokes flow problem, i.e. the flow for a given geometry can be solved, given boundary conditions, without requirements of knowing the flow at any other time. The instantaneous response of velocities to the observed changes in the geometry is hence the response expected from a full dynamic simulation with geometry changes being consistent with observations.

I would also like to see more discussion on this aspect to assess how this could impact the results, especially how the limitations in the model and observations could impact the results.

We hope to address the reviewer's comment about the dependency of our results on uncertainties in the datasets and model parameters in further replies below. In summary, the general limitations of our datasets are now discussed in more detail in AppA (also see Fig.1 above) and the discussion about limitations of our optimization approach has been expanded (see further replies below and App.B in the manuscript).

p.3 l.65: How linear do you expect the different processes to be? Is that something that can be investigated a bit more? Also, with what processes are the impact of grounding line changes included? Same for l.71-72.

We have removed this equation as it is misleading. The terms on the right hand side are not independent quantities, and ΔU cannot be expressed as a sum of dependent quantities. We have removed all references to Eq.(2) from the ms.

p.3 l.74: Despite a lot of limitations, calving has been included in some models for a long time now (Martin et al., 2011) and a growing number of ice flow models are starting to include it at large scale in various forms (Seroussi et al., 2019).

We certainly recognise the use of various calving parameterizations in models, and it is a growing field of research, which is encouraging to see. We have changed the sentence to "...whereas only a limited but growing number of ice flow simulations include parameterizations of calving."

p.3 l.75: I was wondering if this should not be: $\Delta U_a = \Delta U_c = 0$

We have removed all instances of ΔU , ΔU_{Calv} ,... from the introduction, and introduced this notation together with the model experiments in Sect.2, which we believe is more appropriate.

p.3 l.86: What knowledge is referred to here? As mentioned on l.87, it cannot be estimated from observations, I am wondering where this comes from? p.5 Fig.1c: How do you explain the thinning just downstream of the 1996 grounding line?

We have reformulated this sentence, in line with our previous reply. "Knowledge" has been replaced by "Model estimates of".

p.6 l.151: U^* is a little confusing, it might be more clear to list the perturbation experiments or explain a bit more what the asterisk refers to.

We have removed U_ and referred to individual velocities (U_{Calv} ,...) instead.*

p.7 l.167: I would like to see more information on the inversion for A and C. What are the initial values, what are the minimum and maximum values admissible, ... ?

We have added further details about the optimization to App.B

p.7 l.173: What about the thermal regime? What is assumed for that? Many models of Pine Island have been developed over the past few years, so I guess it would not be difficult to use the ice thermal regime from a previous model to get a first guess of the rheology?

In our study we also invert for A over the grounded parts of PIG to include - together with ice temperatures - further factors influencing the ice rheology such as impurities, damage,...(see e.g. the recent study by Lhermitte et al. (2020) who show extensive damage upstream of the GL). We agree that it would be interesting to compare the results with results from a thermodynamic study but since the interpretation of A cannot be based on ice temperature alone, this is also not straightforward. We leave this for a future study.

p.9 l.237: It is not clear which “earlier conclusion” is referred to here.

We have reworded this sentence and restructured this section. The new sentence reads “Figure 3e shows that the retreat of the PIG calving front between 1996 and 2016 accounts for 2% and 13% of the observed flux changes through Gate 1 and 2 respectively, which indicates minor instantaneous changes to the flow upstream of the grounding line.”

p.10 Figure 3e: How gate-dependent are the results? What would happen if gates a few kilometers upstream or downstream were used?

Results are robust with respect to small (~kilometer) shift in the position of the gates. In fact, the gates do not provide any information that isn’t contained in the 2d maps of relative change (e.g. Fig3a-d), but were rather introduced as a convenient way to synthesise the results. The 2d maps provide all the details, and the reviewer is hopefully convinced that results for $(U_{\text{pert}} - U_{96}) / (U_{16} - U_{96})$ (as in Fig3a-d) are spatially coherent and small shifts in the position of the gates will not greatly affect the values in Fig3e.

p.11 l.265: Is that what is expected in that case? Because the effect accumulates in time over 20 years and, even if it is reflected in the 2016 geometry, limitations in model parameters and errors in observations might limit the ability of the model to simulate good instantaneous response.

We are unclear what ‘limitations’ the reviewer refers to. Yes, there might be errors in the 1996 and 2016 ice thickness datasets that influence our results, but it is hard to see how this could account for an additional 72% (Gate1) and 36% (Gate2) of speed-up. Given the excellent agreement between model and DInSAR grounding line locations in both years (see Fig.1), we are confident that both thickness datasets are reasonably accurate. We also note that both thickness datasets have the same variability at small (~km) spatial scales: the 2016 dataset is based on REMA, whereas the 1996 dataset was obtained by subtracting spatially smooth thickness changes (Fig.1). Small-scale errors in the thickness distributions are therefore “consistent” between 1996 and 2016 (i.e. errors related to the REMA dem), and modeled changes in ice velocities are entirely dictated by the spatially smooth thickness changes (i.e. errors in the small-scale thickness distribution cancelling out). We agree that in addition to the geometry, physical properties of the ice (rate factor) and bed (slipperiness) could change between 1996 and 2016, but we believe these have been addressed at length in the manuscript.

p.13 l.308: As mentioned above, you have here two sets of parameters (A2016 with C1996 and A1996 and C2016) that reproduce the 2016 velocity field. There is an infinite number of combinations that can reproduce a given field, so given the limited constraints provided for the inversion of A and C, can we make sure that the results are not dependent on the combination of parameters used?

We agree that the inverse problem is generally ill-posed. To partly address the reviewer’s concern, we have carried out a range of sensitivity tests for model parameters that define the cost function (see our replies to reviewer#1, and replies to your other comments). With regards to the solutions \tilde{A}_{16} and \tilde{C}_{16} of the \mathcal{E}_A and \mathcal{E}_C experiments, these are ‘end members’ that bracket the maximum amount of change required to fully describe the observed speed-up. In reality, it is likely that A and C will evolve simultaneously, and if we assume that our inversions do a perfect job, the original solution (A_{96}, C_{96}) will seamlessly evolve to (A_{16}, C_{16}) . However, if we do not allow C to change over time and keep it fixed at C_{96} , then experiment \mathcal{E}_A diagnoses the required changes to A (solution \tilde{A}_{16}). Similarly, if A is not allowed to change over time and kept fixed at A_{96} , experiment \mathcal{E}_C diagnoses the required changes to C (solution \tilde{C}_{16}). We hope this clarifies the rationale behind these experiments.

p.17 l.397: The limitation of Weertman sliding is mentioned several times, but not really discussed, so it would be nice to see a bit more discussion on that.

In reply to this comment and comments from reviewer#1, we have expanded our discussion about the limitations of a power law sliding at various places in the ms.

p.17 l.403: It should be specified that this is an instantaneous response.

In our study, we let nature carry out the transient evolution of the geometry (i.e we use observations of ice thinning and calving), but use a model to diagnose the corresponding velocity response. This is indeed different from a full transient simulation, where the model simulates both changes

in ice geometry and velocity. Our experiments could be seen as a 'hybrid', whereby changes in ice geometry are prescribed, but the model calculates the changes in flow. We are reluctant to call this 'instantaneous', but we think "...a modern-day ice flow model to diagnose dynamic changes in response to prescribed geometric perturbations" is more accurate.

p.17 l.407: I thought that the results attributing the remaining changes to rigidity or friction were inconclusive as the fields computed were unphysical?

We cannot conclude with certainty that simulated changes in A are indeed unphysical since they could represent damage, changes in fabric etc that are difficult to constrain or observe. We therefore prefer to keep the statement that 'large' changes are needed, without drawing any strong conclusions about their physical validity.

p.18 l.436: So what is used in this region and for the transition?

A linear interpolation of ΔH was used in data sparse regions. Further details have now been included in the App.A, including a new figure (similar to Fig.1 above).

p.19 453: Why use a uniform value of -15 degrees?

This is of course a somewhat arbitrary choice, based on reasonable assumptions about the depth-averaged ice temperature throughout the domain. To test the sensitivity of our results to the choice of prior value, we have performed two sets of additional experiments: (i) inversions were repeated for $A_{\text{prior}} = -25C$ and $A_{\text{prior}} = -5C$; results are shown in Fig.3 above and discussed in an earlier reply to reviewer#1. (ii) inversion were repeated for different values of $(g_a)_A$, which is a pre-multiplier in the amplitude regularization term in the cost function. The value of $(g_a)_A$ effectively controls how 'far' the solution A can deviate from its prior value. Results are shown in Fig.3 and discussed further in our reply to your question below, as well as in an earlier reply to reviewer#1.

p.19 l.463: What are the constraints used for A and C (minimum and maximum values possible)?

For numerical reasons, solutions for A and C are restricted to the interval $[1e-100 \ 1e100]$, but the solution is well within these limits.

p.22 l.505: How about the relative weight for the two parts of the cost function referring to A and C? How are the weights calibrated?

We have not explored relative weights of the A and C pre-multipliers in great detail. In the main experiments, our choice $(g_s)_A = (g_s)_C = 25,000$ was based on the L-curve analysis presented in FigB1. Similarly, we used an L-curve analysis to set $(g_a)_A = (g_a)_C = 1$, which are the pre-multipliers in the amplitude term of the regularization. In fact, we did not elaborate on the g_a values in the main text, but in response to this comment and a related comment by reviewer#2, we have included further details in App.B. We have also carried out experiments for different values of $(g_a)_A \in [0.1, 1, 100]$, whilst keeping $(g_a)_C = 1$ constant, to allow for larger ($(g_a)_A = 0.1$) or smaller ($(g_a)_A = 100$) deviation from A_{prior} . Results for these experiments are shown in Fig.3 above, and described in our replies to reviewer#1.

p.4 l.121: we required - we needed

Done

p.4 l.122: How about grounding line positions?

Changes in GL position are embedded in the differences in ice thickness between 1996 and 2016. However, as the latter were constrained by independent DInSAR GL datasets, we have mentioned GL positions here as well.

p.6 l.160: It would be good to specify where you infer A because different groups use different parts of the domain (entire domain vs floating parts only)

We have added further details about the optimization to App.B

p.8 l.198: missing Delta in front of UCalv or Delta UThinCalv)

Well spotted, thank you.

p.11 l.262: it would be more informative to provide numbers about the difference between Delta UThinCalv and Delta UCalv + Delta UThin rather than just saying they are about the same.

In response to a comment by reviewer#2, we have removed any equations involving ΔU , as these can be confusing. The percentages in Fig.3e provide a quantitative measure for how 'additive' the experiments are. E.g., flux changes through gates 1 and 2 in the ISThin and Thin experiments add up to 27% and 58% respectively, whereas flux changes in CalvThin are 28% and 64% respectively. The flux response in the combined experiment is therefore somewhat larger than the added response of each individual experiment, but we believe these differences are insignificant and not worth elaborating on.

p.11 l.275 and l.277: hypotheses - hypothesis
Done.

p.14 Figure 5d: Would it be possible to add results for more exponents? At least the value for $m=21$ to see the highest change.

We believe that additional panels for higher m are not particularly insightful, as changes relative to the velocity response become smaller for increasing m . In other words, a plot for $m = 21$ would look rather similar to the plot for $m = 13$. This can also be seen from Figure C1a, which shows the asymptotic behaviour in the response for higher values of m .

p.17 l.406: increases - increase
Done.

p.17 l.413: the DOI is missing for now.
A DOI will be provided with the final submission.

p.18 l.338: the finite element method
Done.

p.18 l.438 to l.445: references are missing for the stress balance approximation, inverse capabilities, ...

We have added references to (Hutter, 1983; MacAyeal, 1989) and (MacAyeal, 1992) respectively.

p.20 Figure B1c: It would be good to see the temperature equivalent to the rate factor on top of the rate factor on the colorbar. On all the spatial figures, the x and y axis are ps_x and ps_y , which looks a bit awkward to me, but that's not very important.

We have added temperature labels to the colorbar. We prefer to use ps_x and ps_y in all figures because this identifies the Cartesian coordinates system (polar stereographic).

References

- Barnes, J. M., dos Santos, T. D., Goldberg, D., Gudmundsson, G. H., Morlighem, M., and De Rydt, J.: The transferability of adjoint inversion products between different ice flow models, The Cryosphere Discussions, 2020, 1–32, <https://doi.org/10.5194/tc-2020-235>, 2020.
- Gillet-Chaulet, F., Durand, G., Gagliardini, O., Mosbeux, C., Mougnot, J., Rémy, F., and Ritz, C.: Assimilation of surface velocities acquired between 1996 and 2010 to constrain the form of the basal friction law under Pine Island Glacier, Geophysical Research Letters, 43, 10–311, 2016.
- Hutter, K.: Theoretical Glaciology: Material Science of Ice and the Mechanics of Glaciers and Ice Sheets, Mathematical Approaches to Geophysics, Springer, 1983.
- Joughin, I., Tulaczyk, S., Bamber, J. L., Blankenship, D., Holt, J. W., Scambos, T., and Vaughan, D. G.: Basal conditions for Pine Island and Thwaites Glaciers, West Antarctica, determined using satellite and airborne data, Journal of Glaciology, 55, 245–257, <https://doi.org/10.3189/002214309788608705>, 2009.

- Joughin, I., Smith, B. E., and Schoof, C. G.: Regularized Coulomb friction laws for ice sheet sliding: application to Pine Island Glacier, Antarctica, *Geophysical research letters*, 46, 4764–4771, 2019.
- Lhermitte, S., Sun, S., Shuman, C., Wouters, B., Pattyn, F., Wuite, J., Berthier, E., and Nagler, T.: Damage accelerates ice shelf instability and mass loss in Amundsen Sea Embayment, *Proceedings of the National Academy of Sciences*, 117, 24 735–24 741, <https://doi.org/10.1073/pnas.1912890117>, 2020.
- MacAyeal, D. R.: Large-scale ice flow over a viscous basal sediment: Theory and application to ice stream B, Antarctica, *Journal of Geophysical Research: Solid Earth*, 94, 4071–4087, <https://doi.org/10.1029/JB094iB04p04071>, 1989.
- MacAyeal, D. R.: The basal stress distribution of ice stream E, Antarctica, inferred by control methods, *Journal of Geophysical Research*, <https://doi.org/10.1029/91JB02454>, 1992.
- Rignot, E., Mouginot, J., Morlighem, M., Seroussi, H., and Scheuchl, B.: Widespread, rapid grounding line retreat of Pine Island, Thwaites, Smith, and Kohler glaciers, West Antarctica, from 1992 to 2011, *Geophysical Research Letters*, 41, 3502–3509, 2014.
- Schmeltz, M., Rignot, E., Dupont, T. K., and Macayeal, D. R.: Sensitivity of Pine Island Glacier, West Antarctica, to changes in ice-shelf and basal conditions: A model study, *Journal of Glaciology*, 48, 552–558, <https://doi.org/10.3189/172756502781831061>, 2002.
- Zoet, L. K. and Iverson, N. R.: A slip law for glaciers on deformable beds, *Science*, 368, 76–78, <https://doi.org/10.1126/SCIENCE.AAZ1183>, 2020.

Drivers of Pine Island Glacier ~~retreat from~~ speed-up between 1996 ~~to and~~ 2016

Jan De Rydt¹, Ronja Reese², Fernando S Paolo³, and G. Hilmar Gudmundsson¹

¹Department of Geography and Environmental Sciences, Northumbria University, Newcastle upon Tyne, UK

²Potsdam Institute for Climate Impact Research (PIK), Member of the Leibniz Association, Potsdam, Germany

³Jet Propulsion Laboratory, California Institute of Technology, Pasadena, CA, USA

Correspondence: Jan De Rydt (jan.rydt@northumbria.ac.uk)

Abstract. Pine Island Glacier in West Antarctica is among the fastest changing glaciers worldwide. Over the last two decades, the glacier has lost in excess of a trillion tons of ice, or the equivalent of 3 mm of sea level rise. The ongoing changes are commonly attributed to ocean-induced thinning of its floating ice shelf and the associated reduction in buttressing forces. However, other drivers of change such as large-scale calving, changes in ice rheology and basal slipperiness could play a vital, yet unquantified, role in controlling the ongoing and future evolution of the glacier. In addition, recent studies have shown that mechanical properties of the bed are key to explaining the observed speed-up. Here we used a combination of the latest remote sensing datasets between 1996 and 2016, data assimilation tools and numerical perturbation experiments to quantify the relative importance of all processes in driving the recent changes in Pine Island Glacier dynamics. We show that (1) calving and ice shelf thinning have caused a comparable reduction in ice-shelf buttressing over the past two decades, that (2) simulated changes in ice flow over a viscously deforming bed are only compatible with observations if large and widespread changes in ice viscosity and/or basal slipperiness are taken into account, and that (3) a spatially varying, predominantly plastic bed rheology can closely reproduce observed changes in flow without marked variations in ice-internal and basal properties. Our results demonstrate that in addition to its evolving ice thickness, calving processes and a heterogeneous bed rheology play a key role in the contemporary evolution of Pine Island Glacier.

15 *Copyright statement.* ©2020. This work is distributed under the Creative Commons Attribution 4.0 License.

1 Introduction and motivation

Since the 1990s, satellite measurements have comprehensively documented the sustained acceleration in ice discharge across the grounding line of Pine Island Glacier (PIG, Fig. 1) in West Antarctica (Rignot et al., 2002; Rignot, 2008; Rignot et al., 2011; Mouginot et al., 2014; Gardner et al., 2018; Mouginot et al., 2019b). The changes in flow speed are an observable manifestation of the glacier's dynamic response to both measurable perturbations, such as calving and ice shelf thinning, and poorly constrained variations in physical ice properties and basal sliding. Evidence from indirect observations have indicated that changes in ice shelf thickness have occurred since at least some decades before the 1970s (Jenkins et al., 2010; Smith

et al., 2017; Shepherd et al., 2004; Pritchard et al., 2012). Within the last two decades, thinning of the grounded ice (Shepherd et al., 2001; Pritchard et al., 2009; Bamber and Dawson, 2020), intermittent retreat of the grounding line (Rignot et al., 25 2014), changes in calving front position (Arndt et al., 2018) and the partial loss of ice shelf integrity (Alley et al., 2019) have all been reported in considerable detail. At the same time, numerical simulations of ice flow have confirmed the strong link between ice-shelf thinning, which reduces the buttressing forces, and the increased discharge across the grounding line (~~Schmeltz et al., 2002; Payne et al., 2004; Favier et al., 2014; Arthern and Williams, 2017; Reese et al., 2018; Gudmundsson et al., 2019~~) (Schmeltz et al., 2002; Payne et al., 2004; Joughin et al., 2010; Seroussi et al., 2014; Favier et al., 2014; Arthern and Williams, 2017; Reese et al., 2019).

30 . Due to the dynamic connection between ocean-driven ice shelf melt rates and tropical climate variability (Steig et al., 2012; Dutrieux et al., 2014; Jenkins et al., 2016; Paolo et al., 2018), several model studies have **primarily** focused on the important problem of simulating the response of PIG to a potential anthropogenic intensification of melt. Such external perturbations, in combination with ice-internal feedbacks including the Marine Ice Sheet Instability, can force PIG along an unstable and potentially irreversible trajectory of mass loss (Favier et al., 2014; Rosier et al., 2020). Whereas significant progress has been 35 made in simulating the melt-driven retreat of PIG, less attention has been given to other processes that could affect the force balance and thereby inhibit changes in ice dynamics. Increased damage in the shear margins of the ice shelf, for example, has been reported by Alley et al. (2019) and is known to reduce the buttressing capacity of an ice shelf (Sun et al., 2017). Moreover, a series of recent calving events has caused a sizeable reduction in the extent of the ice shelf, and caused a potential loss of contact with pinning points along the eastern shear margin (Arndt et al., 2018).

40 The relative impact of changes in ice geometry, basal shear stress and/or ice rheology on the dynamics of PIG has previously been emphasised in numerical studies by e.g. Schmeltz et al. (2002); Payne et al. (2004); Gillet-Chaulet et al. (2016); Joughin et al. (2019) and Brondex et al. (2019). In all cases, some combination of thickness changes, ice softening, a reduction in ice shelf buttressing or variations in basal shear stress were required to attain an increase in flow speed comparable to observations. Similar conclusions were reached for other Antarctic glaciers. Based on a comprehensive series of model perturbation 45 experiments, Vieli et al. (2007) suggested that the acceleration of the Larsen B Ice Shelf prior to its collapse in 2002 could not solely be explained by the retreat of the ice shelf front or ice shelf thinning, but required a further significant weakening of the shear margins. Complementary conclusions were reached by Khazendar et al. (2007), who demonstrated the important interdependence of the calving front geometry, a variable ice rheology and flow acceleration based on data assimilation and model experiments for the Larsen B Ice Shelf.

50 In order to comprehensively diagnose the importance of all processes that have contributed to the acceleration of PIG between years 1996 and 2016, this study brings together the latest observations and modelling techniques. We consider how calving, ice shelf thinning, the induced dynamic thinning upstream of the grounding line and potential changes in ice-internal and basal properties have caused a different dynamic response across the ice shelf, the glacier's main trunk, the margins and tributaries. Initial observations indicated that the speed-up of PIG was primarily confined to its fast-flowing central trunk (Rignot et al., 2002; Rignot, 2008), though more complex, spatiotemporal patterns of change have emerged more recently (Bamber and Dawson, 2020). The rapid and spatially diverse acceleration of the flow is an expression of the glacier's dynamic response 55 to changes in the force balance, and it is imperative that numerical ice flow models are capable of reproducing this complex

behavior in response to the correct forcing. In general, the driving stress (τ_d), which depends on the ice thickness distribution, is balanced by resistive stresses that include the basal drag (τ_b), side drag through horizontal shear (τ_W), longitudinal resistive forces (τ_L) and back forces by the ice shelf (τ_{IS}):

$$\tau_d = \tau_b + \tau_W + \tau_L + \tau_{IS}. \quad (1)$$

It is conceivable that each of the terms in Eq. 1 has changed considerably in recent decades, ~~whilst maintaining a balance at all times. This~~ in response to changes in calving front position, ice thickness, ice properties and/or basal slipperiness. The interplay between different changing forces, in combination with the appropriate boundary conditions, underlie the observed ~~dynamical changes of PIG, and form the backbone of any numerical model simulation. In response to changes in the stress balance, modeled changes in ice velocity between time t_0 and t_T can be expanded as follows:-~~

$$\underline{\Delta U(\mathbf{x}) \equiv U_{t_1}(\mathbf{x}) - U_{t_0}(\mathbf{x}) = \Delta U_{Calv} + \Delta U_{Thin} + \Delta U_A + \Delta U_C},$$

~~where terms on the right hand side indicate different contributions to the changes in ice flow, caused by variations in calving front position (ΔU_{Calv}), changes in ice thickness (ΔU_{Thin}), changes in ice properties commonly parameterized by a rate factor A speed-up of PIG (ΔU_A), and changes in basal slipperiness C (ΔU_C). Note that these contributions are not generally independent due to feedbacks within the system, and that only the total sum, ΔU , can be observed directly. The velocity component related to changes in ice thickness, ΔU_{Thin} , generally consists of two contributions: an instantaneous response due to ice shelf thinning, as investigated by e.g. Gudmundsson et al. (2019), and the henceforth denoted by ΔU . Present-day observations of ΔU are generally assumed to be dominated by ice shelf thinning and~~ induced dynamic loss and redistribution of mass upstream of the grounding line. We will separately assess the impact of both components. Present-day observations of ΔU are generally assumed to be dominated by ΔU_{Thin} , whereas other contributions, which includes grounding line retreat and the associated loss of basal traction. Other possible contributions to ΔU , such as ice front retreat or changes in ice viscosity (including damage) or basal slipperiness, remain unquantified and are not generally included in model simulations of future ice flow at decadal to centennial timescales. In particular, temporal changes in ice viscosity and basal sliding are ignored such that $\Delta U_A + \Delta U_C = 0$, whereas only a minority of ice flow models include (simple) parameterizations of calving. These missing processes, if important, could lead to a systematic bias in model projections of future ice loss, or could prompt the use of unrealistically large perturbations in, e.g., τ_{IS} in an attempt to reproduce observed values of ΔU .

In this study we used a regional configuration of the shallow ice stream flow model, $\acute{U}a$ (Gudmundsson, 2020), for PIG to ~~estimate the individual components of~~ diagnose how individual processes (calving, ice thinning and associated grounding line movement, changes in ice viscosity and basal slipperiness) have contributed to ΔU in Eq. ?? between $t_0 = 1996$ and $t_T = 2016$. Results enabled us to quantify the relative importance of each driver of change for the contemporary evolution of PIG, and validate the ability of current-generation ice flow models to reproduce the complex response of PIG to a range of realistic forcings. It is important to note that results were *not* derived from transient simulations of glacier flow based on (uncertain) estimates of the initial model state and external forcings. Instead, the over the period 1996 to 2016. The diagnostic model response to ~~a series of prescribed~~ changes in ice geometry was analysed, based on the latest observations of calving

and ice thinning rates and calving between 1996 and 2016. For each perturbation, changes in the stress balance (Eq. 1) and the associated ice flow response (ΔU_{Calv} and ΔU_{Thin}) were computed. Assuming closure of the velocity budget in Eq. ?? and observed values for ΔU , an estimate for $\Delta U_A + \Delta U_C$ was obtained. Knowledge about the magnitude and spatial distribution of each contribution in Eq. ?? allowed us to

95 Any further discrepancies between modeled and observed changes in velocity were attributed to variations in ice properties, commonly parameterized by a rate factor A , and changes in basal slipperiness. Results enabled us to validate the ability of current-generation ice flow models to reproduce the complex response of PIG to a range of realistic forcings, and to verify whether common model assumptions such as $\Delta U_{\text{Calv}} = 0$ and $\Delta U_A + \Delta U_C = 0$ a static calving front and fixed ice viscosity and basal slipperiness are indeed justified, ~~at least for contemporary flow conditions.~~

Although the aforementioned method provides insights into the individual contribution of geometrical perturbations and changes in ice viscosity and basal slipperiness to overall changes in ice flow, ~~the partitioning between different components of the ΔU budget likely depends~~ results will likely depend on a number of structural assumptions within the ice flow model. In particular, assumptions about the form of the basal sliding law are likely to precondition the partitioning of ΔU . Indeed, ~~previous model~~ Previous studies have shown that different forms of the sliding law, for example, can produce a distinctly different simulated response of PIG to changes in geometry (Joughin et al., 2010; Gillet-Chaulet et al., 2016; Joughin et al., 2019; Brondex et al.

105 ~~Based on the assumption that $\Delta U \approx \Delta U_{\text{Thin}}$, ice thickness (Joughin et al., 2010; Gillet-Chaulet et al., 2016; Joughin et al., 2019; Brondex et al., 2019) and Joughin et al. (2019) showed that a regularized Coulomb law or the plastic limit of a Weertman non-linear viscous power-law provide a better fit between modeled and observed changes in surface velocity along the central flowline of PIG, compared to a commonly used viscous Weertman law~~ Weertman law with a cubic dependency of the sliding velocity on the basal shear stress. Motivated by the above considerations, we explore new ways to derive spatially variable constraints on the form of the sliding law, and thereby provide the first comprehensive, spatially distributed map of basal rheology beneath PIG.

The remainder of this paper is organised as follows. In Sect. 2.1 we introduce the observational datasets used to constrain and validate the ice flow model. Additional details about our data processing methods are provided in App. A. Section 2.2 outlines the experimental design, and provides a summary of the main model components. Further technical details about the model setup and a discussion about the sensitivity of our results to numerical model details are provided in App. B and App. D respectively. Results and an accompanying discussion of all experiments is provided in Sect. 3.1-3.3. Final conclusions are formulated in Sect. 4.

115

2 Data and methods

The first aim of this study is to simulate the dynamic response of PIG to a series of well-defined geometric perturbations ~~between years over the period~~ 1996 ~~and to~~ 2016, and compare model output to observed changes in surface speed over the same time period. As detailed in Sect. 1, geometric perturbations are considered to be observed changes in the calving front position and observed changes in ice thickness. For each perturbed geometry, a diagnostic solution for the surface velocities ~~denoted by U_* , was obtained, where the subscript $*$ refers to individual perturbations~~ was obtained. Since we are primarily

120

interested in the relative contribution of each perturbation to the overall speed-up of PIG between 1996 and 2016, our focus will
125 be on relative changes $\Delta U_*/\Delta U$, where $\Delta U_* = U_* - U_{96}$ with U_* the perturbed velocities, and $\Delta U = U_{16} - U_{96}$. In order to
compute the relative changes in surface flow, two types of model experiment are required: (1) inverse simulation optimization
experiments, which were used to obtain model configurations that are as close as possible to the observed state of PIG in 1996
(U_{96}) and 2016 (U_{16}), and (2) perturbation experiments to obtain estimates of U_* , starting from the 1996 model configuration.
In Sect. 2.1 we list the data sources required for these experiments, whereas a detailed overview of the experimental design is
130 provided in Sect. 2.2.

2.1 Observed changes of Pine Island Glacier between 1996 and 2016

Our study area and model domain encompasses the 135,000 km² grounded catchment (Rignot et al., 2011) and seaward floating
extension of PIG in West Antarctica, as depicted in Fig. 1a. To investigate the physical processes that forced the contemporary
speed-up of the glacier, and its increase in grounding line flux between years 1996 and 2016, we ~~required~~ needed detailed
135 observations of the surface velocity, ice thickness and calving front position for both years.

The surface velocity measurements used in this study were taken from the MEaSURES database (Mouginot et al., 2019a,
b). For 1996, Synthetic Aperture Radar data from the ERS-1/2 mission were processed using interferometry techniques and
combined into a mosaic with effective timestamp 01/01/1996. The MEaSURES velocities for 2016 were based on feature
tracking of Landsat 8 imagery with effective timestamp 01/01/2016. The change in surface speed between both years (denoted
140 by $\Delta U = U_{16} - U_{96}$) is shown in Fig. 1b, and we refer to e.g. Rignot et al. (2014) and Gardner et al. (2018) for a more
comprehensive description of these observations.

Recent estimates of ice thickness were obtained from the BedMachine Antarctica dataset (Morlighem et al., 2020), which
provides both high-resolution surface topography based on the REMA mosaic (Howat et al., 2019) and improved estimates of
bedrock topography using mass conservation methods. The nominal date for this dataset corresponds to the date stamp of the
145 REMA elevation model, which is spatially variable but largely between 2014 and 2018 for PIG. For consistency with previous
notation we refer to the BedMachine Antarctica ice thickness as H_{16} and we assume a uniform timestamp of 01/01/2016.

Ice thickness estimates for 1996, henceforth denoted by H_{96} , were obtained by subtracting measurements of ice thick-
ness change between 1996 and 2016, denoted by ΔH , from H_{16} , i.e. $H_{96} = H_{16} - \Delta H$. Estimates of ΔH were based on a
combination of existing CPOM measurements of thickness change rates (Shepherd et al., 2016) for areas upstream of the 2016
150 grounding line, and newly analyzed data for the floating ice shelf. Detailed information about the latter can be found in App. A.
The resulting values for ΔH , linearly interpolated across the grounding line and in data sparse areas, are shown in Fig. 1c, and
provide the most comprehensive observation-based ice shelf and grounded ice thickness changes for PIG to date.

The grounding line location for H_{16} (blue line in Fig. 1b-c) corresponds to the DInSAR derived grounding line in 2011 from
Rignot et al. (2014), since this is included as a constraint in the generation of the BedMachine Antarctica bed topography. In
155 addition, localized adjustments less than 150 m were made to the bed topography to ensure that the grounding line for H_{96}
(black lines in Fig. 1a-c) corresponds to the DInSAR derived grounding line in 1992-1996 (Rignot et al., 2014).

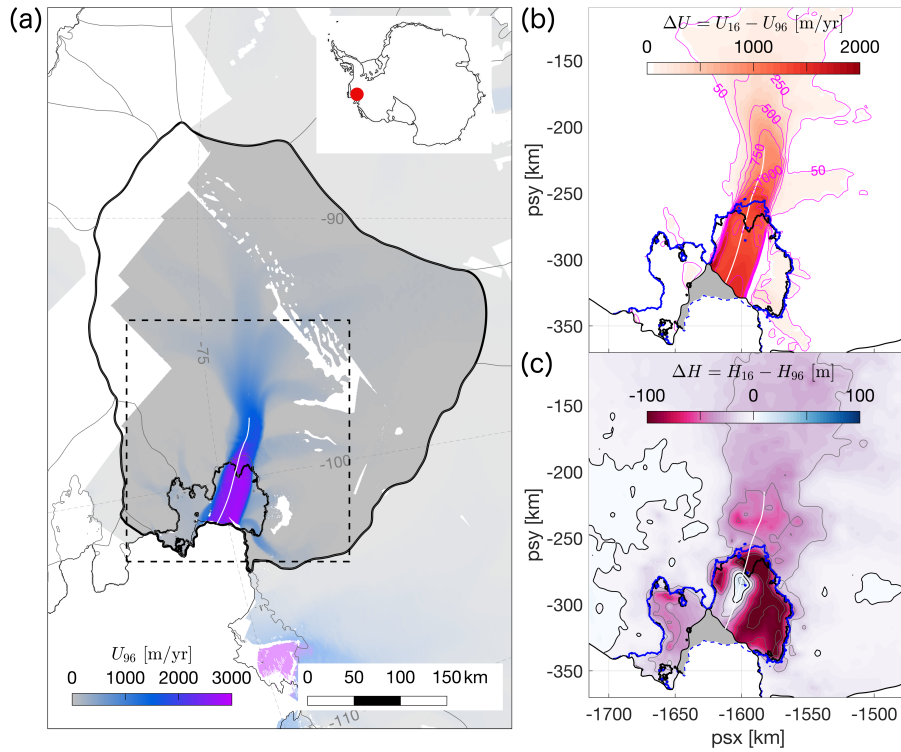


Figure 1. Pine Island Glacier (PIG) and its location in West Antarctica. **(a)** Surface speed of PIG in 1996 in m/yr, as reported by the MEASUREs program (Mouginot et al., 2019a). Solid black outlines delineate the extent of the PIG catchment (Rignot et al., 2011) and 1996 grounding line position (Rignot et al., 2014). The white line along the central flowline indicates the location of the transect in Fig. 2. The dashed rectangle corresponds to the extent of panels **b** and **c**. **(b)** Observed increase in surface speed (Mouginot et al. (2019a), colours and contours in m/yr) and loss of ice shelf extent (grey shaded area) between 1996 and 2016. The blue line indicates the 2011 grounding line (Rignot et al., 2014). **(c)** Total change in ice thickness between 1996 and 2016 (ΔH in m), based on a combination of CPOM data (Shepherd et al., 2016) for the grounded ice and newly analyzed data for the ice shelf (Appendix A). The zero contour is shown in black, other contours in grey are spaced at 20 m intervals.

Alongside the above-listed changes in flow dynamics and ice thickness, the calving front of PIG retreated by up to 30 km between 1996 and 2016 during a succession of large-scale calving events; see e.g. Arndt et al. (2018). We traced the calving front positions in 1996 and 2016 from cloud free Landsat 5 and Landsat 8 panchromatic band images with timestamps 18/02/1997 and 25/12/2016 respectively. Both outlines are included in Fig. 1b-c, and the ice shelf area that was lost between 1996 and 2016 is shaded in grey.

2.2 Experimental design

We discuss the numerical experiments required to obtain an optimal model configuration for the state of PIG in 1996 (U_{96}) and 2016 (U_{16}) in Sect. 2.2.1. Experiments that provide estimates of U_* for a series of observed perturbations in the geometry of PIG are introduced in Sect. 2.2.2. Experiments that simulate changes in the rate factor or basal slipperiness are detailed in Sect. 2.2.3.

2.2.1 Inverse Optimization experiments

We explicitly solved the stress balance in year 1996 (an analogous routine was applied for 2016) by assimilating the known ice thickness (H_{96}), calving front position and surface velocity (U_{96}) in the shallow ice stream (SSA) model \acute{U} a (Gudmundsson et al., 2012; Gudmundsson, 2020). This ‘data assimilation’ or ‘inverse optimization’ step is commonly adopted in glaciology (see MacAyeal (1992) for one of the earliest examples) to minimize the misfit between modeled and observed surface velocities through the optimization of uncertain physical parameters. The inverse optimization capabilities of \acute{U} a (further details in App. B) were used to optimize the uncertain spatial distribution of the rate factor, A , and basal slipperiness, C . These physical parameters define the constitutive model and the relationship between basal shear stress τ_b and basal sliding velocity U_b respectively:

$$\dot{\epsilon} = A\tau_E^{n-1}\tau, \quad (2)$$

$$\tau_b = C^{-1/m} \|U_b\|^{\frac{1}{m}-1} U_b \quad (3)$$

Glen’s law, Eq. 2, relates the strain rates $\dot{\epsilon}$ to the deviatoric stress tensor τ . A creep exponent $n = 3$ was used throughout this study. Equation 3 is known as a Weertman sliding law (Weertman, 1957), and describes a linear viscous, non-linear viscous or close-to plastic bed rheology for $m = 1$, $m > 1$ and $m \gg 1$ respectively. Throughout this study, a range of values for m are considered, as specified below. For each m we performed a new inversion for A and C , ~~which caused small variations in τ_b between cases, but produced an optimal fit between modeled and observed surface velocities in each case. This method differs from other studies, e.g. Joughin et al. (2019), who performed a single inversion for $m = 1$, and obtained C for different values of m by solving Eq. 3 under the assumption that τ_b remains constant. We consider our approach to be more appropriate for this study, as our focus is primarily on an accurate model representation of the surface flow (e.g. Eq. ??). Results for A and C for results for $m = 3$ are provided in Appendix App. B. The outcome of the inverse step is a best estimate for each term optimization step is an optimal estimate for A and C that best fits the stress balance in Eq. 1, based on for given observations of geometry and surface velocity of PIG, associated measurement errors and assumptions about the prior values of A and C in year 1996. Analogous results were obtained for 2016.~~

2.2.2 Geometric perturbation experiments

In the second step we carried out a series of numerical perturbation experiments, starting from the 1996 model configuration, to simulate the impact of observed changes in geometry on the flow of PIG. The rate factor and basal slipperiness were kept fixed

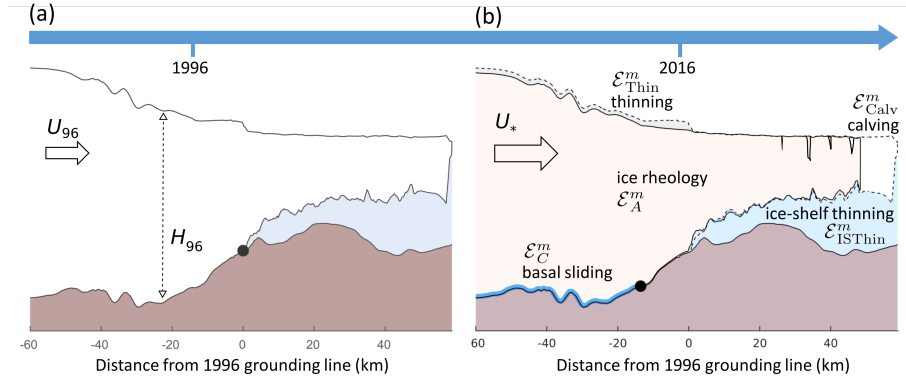


Figure 2. Overview of changes along the Pine Island Glacier centerline from (a) year 1996 to (b) year 2016. Increased ice flow is driven by a combination of calving, ice-shelf thinning and dynamic thinning with movement of the grounding line, as well as changes in basal sliding and ice rheology. Transects of the geometry are based on observations along the flowline indicated in Fig. 1; black dots indicate the respective grounding line positions in both years. Crevasses are introduced for illustration purposes only and do not strictly correspond to observed features. The importance of each ‘driver of change’ was investigated in a series of numerical perturbation experiments, denoted by \mathcal{E}_*^m in panel b, with m indicating the sliding exponent and $*$ the respective experiment described in section 2.2.

to their 1996 values for areas that remain grounded. In areas that unground due to ice thinning, the basal traction reduces to zero and slipperiness values becomes irrelevant. For each perturbation, the modified force balance (Eq. 1) and corresponding surface velocities, U_* , were diagnosed within $\acute{U}a$. Experiments are referred to as \mathcal{E}_*^m with a variable subscript to indicate the type of perturbation and a superscript to specify the value of the sliding exponent m . Experiments were carried out for a range of exponents so we leave m unspecified for now.

- $\mathcal{E}_{\text{Calv}}^m$. Changes in the calving front location were prescribed to reflect the loss of ice shelf between 1996 and 2016 (see Fig. 1b-c). All model grid elements downstream of the 2016 calving front (grey shaded area in Fig. 1b) were deactivated, whilst elements upstream of the 2016 calving front remained fixed to avoid numerical interpolation errors. All other model variables were kept fixed.
- $\mathcal{E}_{\text{ISThin}}^m$. Changes in ice shelf thickness were prescribed, corresponding to observed thinning of the ice shelf between 1996 and 2016 (Fig. 1c). Note that the calving front and grounding line location did not change in this experiment. This experiment is similar to previous studies, e.g. (Reese et al., 2018; Gudmundsson et al., 2019).
- $\mathcal{E}_{\text{Thin}}^m$. Observed changes in both the floating and grounded parts of PIG were prescribed. This caused the grounding line to move from its 1996 position (black line in Fig. 1b-c) to the 2016 position (blue line in Fig. 1b-c).
- $\mathcal{E}_{\text{CalvThin}}^m$. Combined changes in calving front position (as in $\mathcal{E}_{\text{Calv}}^m$), and thinning (as in $\mathcal{E}_{\text{Thin}}^m$) were prescribed.

A schematic overview of the experiments is provided in Fig. 2. While $\mathcal{E}_{\text{Calv}}^m$ allows us to assess the time-integrated-instantaneous impact of calving between 1996 and 2016 (ΔU_{Calv}), and the experiment $\mathcal{E}_{\text{ISThin}}^m$ simulates the instantaneous response to to-

210 tal changes in ice shelf thickness between 1996 and 2016 (ΔU_{ISThin}), ~~both experiments ignore the time-dependent, dynamic response of the upstream grounded ice. These.~~ The separate perturbations make it possible to disentangle ~~the~~ changes in ice shelf buttressing caused by each process, and hence their relative importance for driving the transient evolution of the flow. However, both experiments ignore the time-dependent, dynamic response of the upstream grounded ice and the associated loss of basal traction due to grounding line movement. Dynamic thinning of grounded ice, as well as migration of the grounding
 215 line, is included in the experiments $\mathcal{E}_{\text{Thin}}^m$, which allows us to determine the full response to changes in ice thickness (ΔU_{Thin}). Finally, the experiment $\mathcal{E}_{\text{CalvThin}}^m$ combines both calving and ice thinning, and thereby accounts for all geometric ~~perturbation,~~ and provides a spatial distribution of $\Delta U_{\text{Thin}} + U_{\text{Calv}}$ perturbations.

2.2.3 Estimates of changes in A and C

Later on we show that geometric perturbations alone are not able to fully reproduce the observed patterns of speed-up across
 220 the PIG catchment, i.e. $\Delta U \neq \Delta U_{\text{CalvThin}}$. It is conceivable that, along with the evolving geometry, variations in ice and basal properties have contributed to the changes in flow between 1996 and ~~2016, i.e. $\Delta U_A + \Delta U_C \neq 0$.~~ 2016. Indeed, feedback mechanisms are likely to cause an important interdependence between geometry-induced changes in ice flow, shear softening and/or changes in basal shear stress. Reliable observations of changes in rheology and basal properties are not available, but numerical inverse optimization simulations can provide valuable insights into their evolution. We used the inverse method as
 225 described in Sect. 2.2.1 and App. B to estimate necessary bounds on the magnitude and spatial distribution of changes in A and C that are required beside the geometrical changes already applied, to produce the speed-up of PIG between 1996 and 2016. Changes in A and C are treated separately.

- \mathcal{E}_A^m . The aim of this experiment is to determine possible changes in the rate factor between 1996 (A_{96}) and 2016 (A_{16}). A_{96} was previously obtained in part 1 (inverse optimization step) of the experimental design. To estimate A_{16} , an inverse
 230 optimization problem was solved for the 2016 PIG geometry (H_{16}) and velocities (U_{16}), but using a cost function that was minimized with respect to A only. The slipperiness C was kept fixed to its 1996 solution.
- \mathcal{E}_C^m . This experiment is analogous to \mathcal{E}_A^m , but the cost function in the inverse problem was optimized with respect to C only, whereas the rate factor A was kept fixed to its 1996 solution.

3 Results and discussion

235 3.1 Ice dynamics response to changes in geometry between 1996 and 2016

We present results for the first set of perturbation experiments, which simulate the impact of observed changes in geometry on the flow of PIG. As detailed in section 2.2.2, perturbations are split between four separate cases: 1) calving ($\mathcal{E}_{\text{Calv}}^3$), 2) thinning of the ice shelf ($\mathcal{E}_{\text{ISThin}}^3$), 3) thinning of the ice shelf and grounded ice ($\mathcal{E}_{\text{Thin}}^3$), and which includes associated movement of the grounding line and changes in basal traction, and 4) the combined impact of all ~~observed geometrical changes the above~~
 240 ($\mathcal{E}_{\text{CalvThin}}^3$). We did not previously specify the value of the sliding exponent, however, here we set $m = 3$, which is a commonly

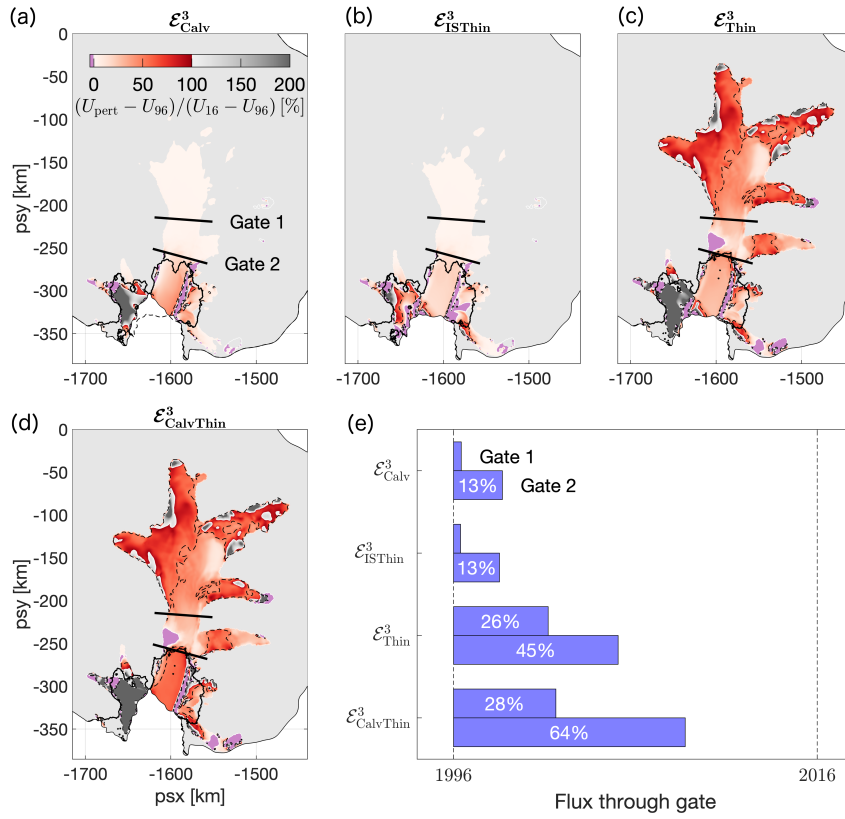


Figure 3. Modelled changes in surface speed compared to 1996 for prescribed perturbations of the Pine Island Glacier geometry. **(a)** Retreat of the calving front, **(b)** thinning of the ice shelf, **(c)** thinning of the ice shelf and grounded ice, including grounding line retreat, **(d)** calving and thinning combined. For each perturbation, the modeled change in speed ($U_* - U_{96}$) is expressed as a percentage of the observed speed-up between 1996 and 2016 ($U_{16} - U_{96}$). Dashed black lines correspond to the 50% contour. Panel **(e)** shows the percentage of the observed flux changes through Gate 1 and 2 that can be explained by the respective perturbations. The simulated impact of calving and thinning in experiment $\mathcal{E}_{CalvThin}^3$ ~~underestimates measured flux changes by 72%~~ only represent 28% and 64% of the measured flux changes respectively. Possible explanations for the unexplained increase in flow speed are provided in Sect. 3.2 and Sect. 3.3 .

adopted value in ice flow modeling and describes a non-linear viscous, rate-strengthening bed rheology. We will explore results for different values of m in Sect. 3.3.

245 Results for the relative change in surface speed for each of the above perturbations are presented in Fig. 3a-d. Flux gates provide an alternative, aggregated way to convey the results. In addition to spatial maps of relative velocity changes, we present flux calculations for two gates perpendicular to the flow within the central part of PIG, as displayed in Fig. 3a. Gate 1 is situated about 50 km upstream of the 2016 grounding line and captures the inland propagation of changes in ice flow. Gate 2 approximately coincides with the 2016 grounding line position and captures changes in grounding line flux, which is a direct measure for PIG's increasing contribution to sea level rise, and an important indicator of change.

Calving as simulated in $\mathcal{E}_{\text{Calv}}^3$ causes changes in flow speed that are predominantly restricted to the outer ice shelf, where it accounts for up to 50% of the observed speed-up between 1996 and 2016 (Fig. 3a). A smaller dynamical impact is also felt upstream of the grounding line, caused by the calving-induced reduction in ice shelf buttressing and mechanical coupling between the floating and grounded ice. Along the central, fast-flowing trunk of PIG, calving typically accounts for less than 10% of the observed speed-up, with little or no effect on the dynamics of the upstream tributaries. Our results are consistent with earlier work by Schmeltz et al. (2002); their calving scenario “part 2”. The only area with negative relative changes in our simulation is the western shear margin of the ice shelf, where modeled and observed changes in flow speed have the opposite sign. Extensive damage has caused this margin to migrate and significant interannual variations in flow speed have been reported by ~~Christianson et al. (2016)~~ Christianson et al. (2016); Lhermitte et al. (2020), a process that is not captured by this experiment.

~~Flux-gates provide an alternative, aggregated way to convey the above results. We present flux calculations for two gates perpendicular to the flow within the central part of PIG, as displayed in Fig. 3a. Gate 1 is situated about 50 upstream of the 2016 grounding line and captures the inland propagation of changes in ice flow. Gate 2 approximately coincides with the 2016 grounding line position and captures changes in grounding line flux, which is a direct measure for PIG’s increasing contribution to sea level rise, and an important indicator of change.~~ Figure 3e shows that calving accounts for 2% and 13% of the observed flux changes through Gate 1 and 2 respectively. ~~This supports the earlier conclusion that the retreat of the PIG calving front between 1996 and 2016 has caused only~~, which confirm the minor instantaneous changes to the flow upstream of the grounding line.

Thinning of the ice shelf as simulated in experiment $\mathcal{E}_{\text{Thin}}^3$ $\mathcal{E}_{\text{ISThin}}^3$ induces a flow response that is similar to calving, as shown in Fig. 3b, and indicates that calving and ice shelf thinning have caused a similar perturbation in the buttressing forces. The largest percentage changes are found on the ice shelf, and are typically less than 25%, while the relative flux changes through Gate 1 and 2 are identical to the calving experiment (Fig. 3e). Ice shelf thinning is generally accepted to be the main driver of ongoing mass loss of PIG, and patterns of ice shelf thinning elsewhere in Antarctica are strongly correlated to observed changes in grounding line flux (Reese et al., 2018; Gudmundsson et al., 2019). However, the force perturbations that result from ice shelf thinning alone, in particular the instantaneous reduction in back forces τ_{IS} , are not sufficient to explain the magnitude of observed changes in upstream flow, consistent with previous studies (Seroussi et al., 2014; Joughin et al., 2010, 2019). Indeed, experiment $\mathcal{E}_{\text{ISThin}}^3$ demonstrates that the direct and instantaneous contribution of ice shelf thinning to observed changes in grounding line flux are less than 25%. Instead, time-evolving changes in geometry and mass redistribution upstream of the grounding line, which may cause grounding line retreat and associated loss of basal traction, play a significant role in increasing the dynamic response of the glacier. These dynamic changes, caused indirectly by changes in the calving front position and ice shelf thinning, were not captured by the experiments $\mathcal{E}_{\text{Calv}}^3$ and $\mathcal{E}_{\text{ISThin}}^3$, but are considered in experiment $\mathcal{E}_{\text{Thin}}^3$.

In experiment $\mathcal{E}_{\text{Thin}}^3$ we prescribed the time integrated change in ice thickness between 1996 and 2016 for both the floating ice shelf and upstream grounded ice. This perturbation incorporates the observed recession of the PIG grounding line between 1996 and 2016. The combined reduction in ice shelf buttressing, loss of basal friction due to grounding line retreat and changes in driving stress caused a significant and far-reaching impact on the flow, as displayed in Fig. 3c. Modeled changes on the

ice shelf are consistent with and similar in amplitude to $\mathcal{E}_{\text{ISThin}}^3$. Upstream of the grounding line, modeled changes relative to observations are between 25% and 50% along the central trunk and up to 100% along the tributaries. In addition, results demonstrate that glacier-wide changes in ice thickness account for 26% and 45% of the observed changes in ice flux through Gate 1 and 2 respectively (Fig. 3e).

In the final perturbation experiment, $\mathcal{E}_{\text{CalvThin}}^3$, the combined effect of calving and changes in ice thickness were simulated. Modeled versus observed changes in surface speed are shown in Fig. 3d. The spatial pattern is consistent with previous experiments, and the amplitude of the response is approximately equal to the added response of experiments $\mathcal{E}_{\text{Calv}}^3$ and $\mathcal{E}_{\text{Thin}}^3$, i.e. $\Delta U_{\text{CalvThin}} \approx \Delta U_{\text{Calv}} + \Delta U_{\text{Thin}}$. The corresponding percentage changes in ice flux through Gate 1 and 2 are 28% and 64% respectively, whereas modeled changes in flow across the grounding line proper account for about 75% of the observed increase in flux between years 1996 and 2016. Although this experiment prescribes all observed changes in PIG geometry over the observational period, model simulations are unable to capture a significant percentage of the observed speed-up. This is most noticeable along the fast-flowing central trunk upstream of the grounding line, whereas discrepancies decrease along the slow-flowing tributaries in the high catchment. We also note that in one area between Gate 1 and 2, modeled and observed changes in surface speed have opposite signs.

Although it is not unexpected to find differences between diagnostic model output and observations, the consistently suppressed response of the model to realistic perturbations in ice geometry is indicative of a structural shortcoming within our experimental design. Indeed, results show that for a non-linear viscous bed rheology described by a Weertman sliding law with constant sliding coefficient $m = 3$, changes in ice geometry alone cannot explain the complex and spatially variable pattern of speed-up over the observational period, i.e. $\Delta U \neq \Delta U_{\text{CalvThin}}$. In the remainder of this study, two possible hypotheses are analyzed that enable to close the gap between geometry-induced changes in ice flow and the observed speed-up of PIG. The first hypotheses hypothesis, which is considered in section 3.2, assumes that bed deformation can indeed be described by a non-linear viscous power law with $m = 3$, but further temporal variations in ice viscosity and/or basal slipperiness are required in addition to changes in geometry: $\Delta U = \Delta U_{\text{CalvThin}} + \Delta U_A + \Delta U_C$. The second, alternative hypotheses, discussed in section 3.3, assumes that internal properties of the ice and bed have not significantly changed between years 1996 and 2016, i.e. $\Delta U_A + \Delta U_C \approx 0$, but a different physical description of the basal rheology is required instead.

3.2 Changes in the rate factor and basal slipperiness between years 1996 and 2016

In transient model simulations of large ice masses such as Antarctica’s glaciers and ice streams, it is common to assume that the advection of A with the ice, or changes due to temperature variations and fracture as well as changes in basal slipperiness C , exert a second-order control on changes in ice flow. As such, temporal variability in A and C are often ignored, based on the assumption that these changes are sufficiently slow and do not significantly affect the flow on typical decadal to centennial timescales under consideration. The aim of experiments \mathcal{E}_A^3 and \mathcal{E}_C^3 , as outlined in section 2.2.3, is to establish whether this is a valid assumption, or whether previously ignored changes in A and/or C can provide a realistic explanation for the discrepancy between simulated and observed changes in the surface speed of PIG in the geometric experiment $\mathcal{E}_{\text{CalvThin}}^3$. Experiment \mathcal{E}_A^3 assumes that, in addition to changes in geometry, temporal variations in A alone are able to explain the significant **increases**

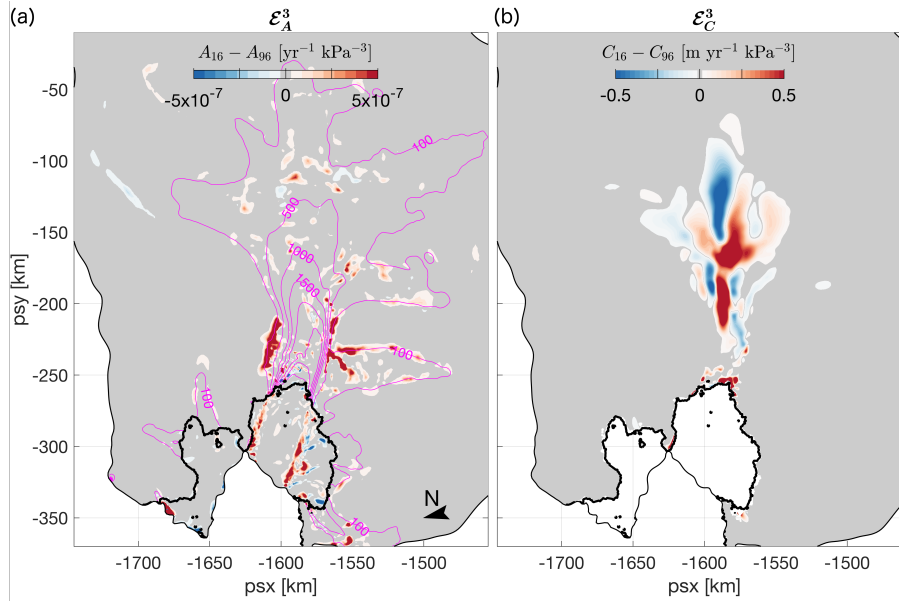


Figure 4. (a) Results for the \mathcal{E}_A^3 experiment: changes in the rate factor A required to fully explain the reproduce observed changes in surface speed of the ice shelf and grounded ice between years 1996 and 2016. The sliding exponent $m = 3$ and basal slipperiness C are-were kept fixed between 1996 and 2016. for grounded areas. Magenta contours (in m/yr) correspond to the surface speed in 2016. (b) Results for the \mathcal{E}_C^3 experiment: changes in the basal slipperiness C required to explain the observed increase in surface speed of the grounded ice between 1996 and 2016. The rate factor A is assumed constant between 1996 and 2016.

increase in flux that were unaccounted for in previous experiments. Alternatively, \mathcal{E}_C^3 assumes that, in addition to changes in geometry, temporal variations in C alone are able to explain the discrepancy in section 3.1 between the modeled and observed speed-up. In line with previous experiments we assume a Weertman sliding law with $m = 3$. The results for both experiments are summarized in Fig. 4.

Changes in A (Fig. 4a), needed to fully reproduce the speed-up of PIG between years 1996 and 2016, are spatially coherent and predominantly positive. This suggests a reduction in ice viscosity between 1996 and 2016, either as a result of localized heating, enhanced damage within the ice column or changes in anisotropy. The largest changes are found in distinct geographical areas: a localized increase within the shear margins of the ice shelf, and a more widespread increase along the slower-moving flanks (magenta contours in Fig. 4a indicate surface speed in 2016) of the main glacier and westernmost tributary, about 20 km upstream of the 2016 grounding line. Changes within the ice shelf shear margins are consistent with their increasingly complex and damaged morphology, as is apparent from satellite images (Alley et al., 2019). Weakening of the ice in these areas accounts-is sufficient to account for the remaining 50% of observed changes in ice-shelf speed-up that could not previously be explained by calving and ice shelf thinning alone (experiment $\mathcal{E}_{\text{CalThin}}^3$). Projected changes in A along the flanks of the upstream glacier, on the other hand, are more ambiguous. Values in excess of $10^{-7} \text{ yr}^{-1} \text{ kPa}^{-3}$ correspond to an equivalent increase in ‘ice’ temperature by up to 40°C . This is nonphysical unless (part of) the change is attributed to damage

or evolution of the ice fabric. Based on our analysis of Sentinel and Landsat satellite images, there is no obvious indication of recent changes in the surface morphology in these areas. Either significant and wide-spread changes in the thermal and mechanical properties have occurred beneath the surface, or the observed speed-up and thinning in these areas, as previously reported by Bamber and Dawson (2020), cannot be convincingly attributed to changes in the rate factor.

Alternatively, temporal changes in C can be invoked to explain the discrepancies between modeled and observed changes in surface speed between years 1996 and 2016. Results presented in Fig. 4b suggest that a complex and widespread pattern of changes in the slipperiness is required across an extensive portion of PIG's central basin and its upper catchment. Despite the complex and poorly understood relationship between C and quantifiable physical properties of the ice/bed interface, it is difficult to understand how any single process or combination of physical processes could be responsible for the large and widespread changes in C over a time period of two decades. Further information, such as a timeseries of maps similar to Fig. 4b, can potentially be used to test the robustness of this result and provide further insights into the physical processes that could control such changes. This is the subject of future research.

We note that in the \mathcal{E}_C^3 experiment, velocities on the floating ice shelf were largely unaffected by changes in C , and remained significantly slower than observations (not shown). In contrast, changes in the rate factor were able to fully account for the speed-up of the ice shelf. On the other hand, large variations in A were needed to explain the changes in ice dynamics along the slow-moving flanks of PIG (Fig. 4a), whereas only small changes in C less than $10^{-3} \text{ yr}^{-1} \text{ kPa}^{-3} \text{ m}$ were required to explain this behaviour. It is therefore conceivable that, in addition to PIG's evolving geometry, an intricate combination of changes in both the rate factor and basal slipperiness are required to explain the glacier's complex and spatially-diverse patterns of speed-up over the last two decades. It is however not straightforward to disentangle these processes in the current modeling framework.

3.3 Evidence for a heterogeneous bed rheology

The relationship between changes in geometry and the dynamic response of a glacier crucially depends on the mechanical properties of the underlying bed and subglacial hydrology. So far, we have assumed that basal sliding can be represented by a ~~viscous power law~~ non-linear viscous power-law with spatially uniform stress exponent $m = 3$ (see Eq. 3). A ~~viscous power law~~ rheology is particularly suitable for the description of hard-bedded sliding without cavitation (Weertman, 1957), but missing processes such as variations in effective pressure or the deformation of a subglacial till layer with a maximum shear (yield) stress could be important limitations. Some evidence has been provided for plastic bed properties underneath ice streams either from observations (Tulaczyk et al., 2000; Minchew et al., 2016) or laboratory experiments (Zoet and Iverson, 2020). Most recently, Gillet-Chaulet et al. (2016), Brondex et al. (2019) and Joughin et al. (2019) used numerical simulations to show that different sliding laws can cause a distinctly different dynamical response of PIG to changes in geometry, and observed changes in surface velocity were best reproduced for sliding exponents $m \gg 1$ or using a hybrid law that combines ~~Weertman power-law~~ with Coulomb sliding. Although the results are compatible with a plastic bed underlying the central trunk of PIG, no constraints on the spatial variability in basal rheology were derived.

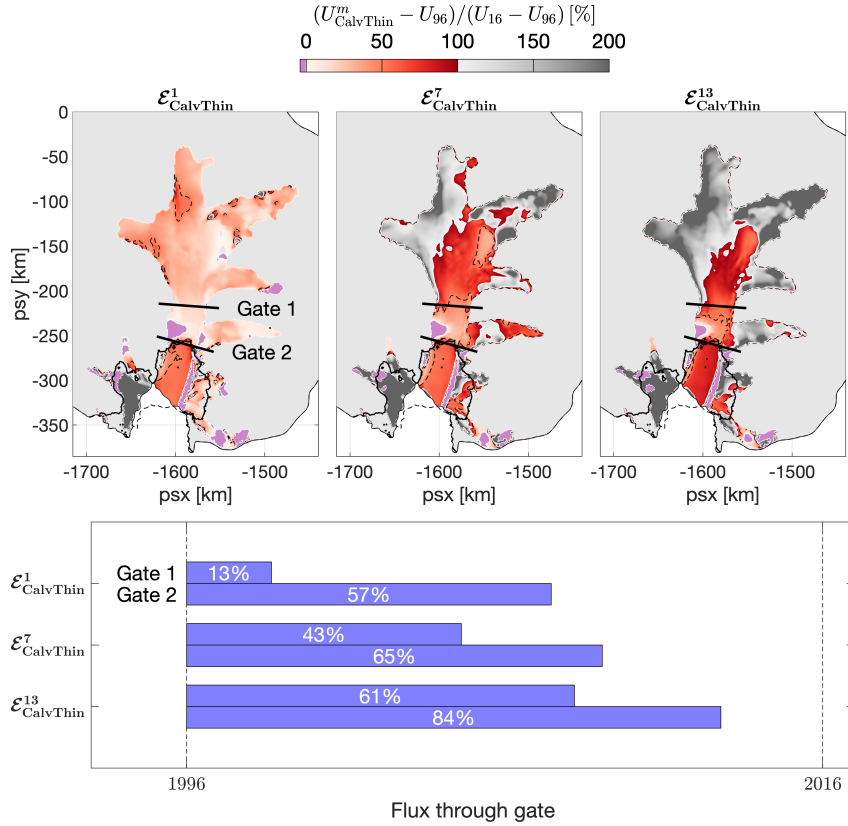


Figure 5. Dependency of simulated-versus-observed changes in surface speed on the sliding law exponent: (a) $m = 1$, (b) $m = 7$ and (c) $m = 13$. Dashed black lines correspond to the 50% contour. Larger values of m cause an increased response of the modeled surface speed to geometrical changes (calving, thinning and grounding line retreat). For $m > 3$, the modeled response of slow-flowing ice in the upstream catchment exceeds observed changes by more than 2-fold, whereas for $m = 13$, modeled changes of the fast-flowing central trunk are still smaller than observed changes. (d) Changes in flux through Gate 1 and 2 as a percentage of observed changes for $m = 1, 7$ and 13 .

In order to quantify how different values of the sliding exponent affect the sensitivity of PIG to changes in geometry across the catchment, we repeated perturbation experiments $\mathcal{E}_{\text{CalvThin}}^m$ for a range of sliding law exponents, from $m = 1$ to $m = 21$ at increments of two. Results for $m = 1, 7$ and 13 are shown in Fig. 5. A linear rheology induces a simulated response to calving and thinning that explains less than 50% of the observed changes everywhere. For $m = 7$, relative changes in flow speed exceed 100% along significant portions of the slower-flowing tributaries. For $m = 13$, which effectively corresponds to a plastic rheology, the modeled response overshoots observations by more than 100% in most areas, except along the main glacier, where the response approaches 100%. Across the model domain, a significant positive correlation exists between m and relative velocity changes, indicating a stronger dynamic response to perturbations in geometry with increasing values of m . This finding is in agreement with Gillet-Chaulet et al. (2016) and Joughin et al. (2019), however our maps show that no

375 single, spatially uniform value of the sliding exponent is able to produce a good match between model output and observations across the entire catchment.

The positive correlation between the flow response and m is an inherent property of the adopted physical description of glacier dynamics. For the shallow ice stream approximation with a non-linear [Weertman-viscous](#) sliding law, the first-order response of the surface velocity, δU , to small perturbations in surface elevation, δS , was previously determined by Gudmundsson
380 (2008) and depends on m in the following non-linear way :

$$\delta U \equiv |\mathcal{T}_{US}(m)|\delta S = \frac{f_1 m}{m + f_2} \delta S. \quad (4)$$

The transfer amplitude $|\mathcal{T}_{US}|$ contains complicated positive functions f_1 and f_2 that generally depend on the wavelength of the surface perturbation, geometrical factors such as the local bed slope, and the basal slipperiness C . Further details are provided in App. C. Despite the simplifying assumptions that underlie the analytical expression of $|\mathcal{T}_{US}|$ obtained by Gudmundsson
385 (2008), results from our simulations $\mathcal{E}_{\text{CalvThin}}^{m_i}$, $m_i \in \{1, 3, \dots, 21\}$, indicate that Eq. 4 is also applicable to the more complex setting of PIG. Indeed, as explained in detail in App. C, we found that across a large portion of the PIG catchment, the transfer amplitude $|\mathcal{T}_{US}|$ provides a suitable model to describe the dependency of the relative velocity changes $\Delta U_{\text{CalvThin}}/\Delta U$ on m . The parameters f_1 and f_2 were treated as spatially variable fields, and best estimates for $f_1(\mathbf{x})$ and $f_2(\mathbf{x})$ were obtained by minimizing the misfit between $\frac{f_1(\mathbf{x})m}{m+f_2(\mathbf{x})}$ and $\frac{\Delta U_{\text{CalvThin}}^{m_i}}{\Delta U}(\mathbf{x})$ with $m_i \in \{1, 3, \dots, 21\}$.

390 Given the non-linear dependency of $\Delta U_{\text{CalvThin}}/\Delta U$ on m with known fields $f_1(\mathbf{x})$ and $f_2(\mathbf{x})$, one can derive an ‘optimal’ spatial distribution of the sliding exponent, $m_{\text{optimal}}(\mathbf{x})$, such that $\Delta U_{\text{CalvThin}}/\Delta U = 100\%$ everywhere, namely

$$m_{\text{optimal}}(\mathbf{x}) = \frac{100f_2(\mathbf{x})}{f_1(\mathbf{x}) - 100} \frac{f_2(\mathbf{x})}{f_1(\mathbf{x}) - 1}. \quad (5)$$

By construction, the variable sliding exponent $m_{\text{optimal}}(\mathbf{x})$ enables to reproduce 100% of the observed speed-up of PIG in response to calving and ice thickness changes. The results, depicted in Fig. 6a, indicate that plastic bed conditions ($m \gg 1$)
395 prevail across most of the fast-flowing central valley and parts of the upstream tributaries. Values generally increase towards the grounding line, whilst linear or weakly non-linear bed conditions are consistently found in the slow-flowing inter-tributary areas. This finding is compatible with the presence of a weak, water saturated till beneath fast-flowing areas of PIG, and hard bedrock or consolidated till between tributaries (Joughin et al., 2009). [The transition to lower exponents in areas with slower flow \(\$< 600 \text{ m a}^{-1}\$ \) is also consistent with results based on a Coulomb-limited sliding law, which produces Coulomb plastic behaviour at speeds \$> 300 \text{ m a}^{-1}\$ and weakly non-linear viscous sliding at slower speeds \(Joughin et al., 2019\).](#)
400

Two interesting properties of the regression model in Eq. 4 are worth noting. Firstly, for $m \rightarrow \infty$, the function $|\mathcal{T}_{US}|$ approaches a horizontal asymptote with limit equal to f_1 . As a consequence, the associated solution for m_{optimal} diverges to ∞ for locations x where $f_1(x) = 100$, and becomes negative where $f_1(x) < 100$. In these areas, indicated by black dots in Fig. 6a,
405 no non-negative, finite value of m exists such that $\Delta U_{\text{CalvThin}}(x)/\Delta U(x) = 100\%$, and conventional Weertman sliding is unable to fully reproduce the observed flow changes in response to thickness changes and calving. Either a different form of the sliding law is required, or additional changes in the rate factor A and/or basal slipperiness C are needed. These findings are the subject of a forthcoming study. Our second observation concerns locations where ΔU either contains significant measurement

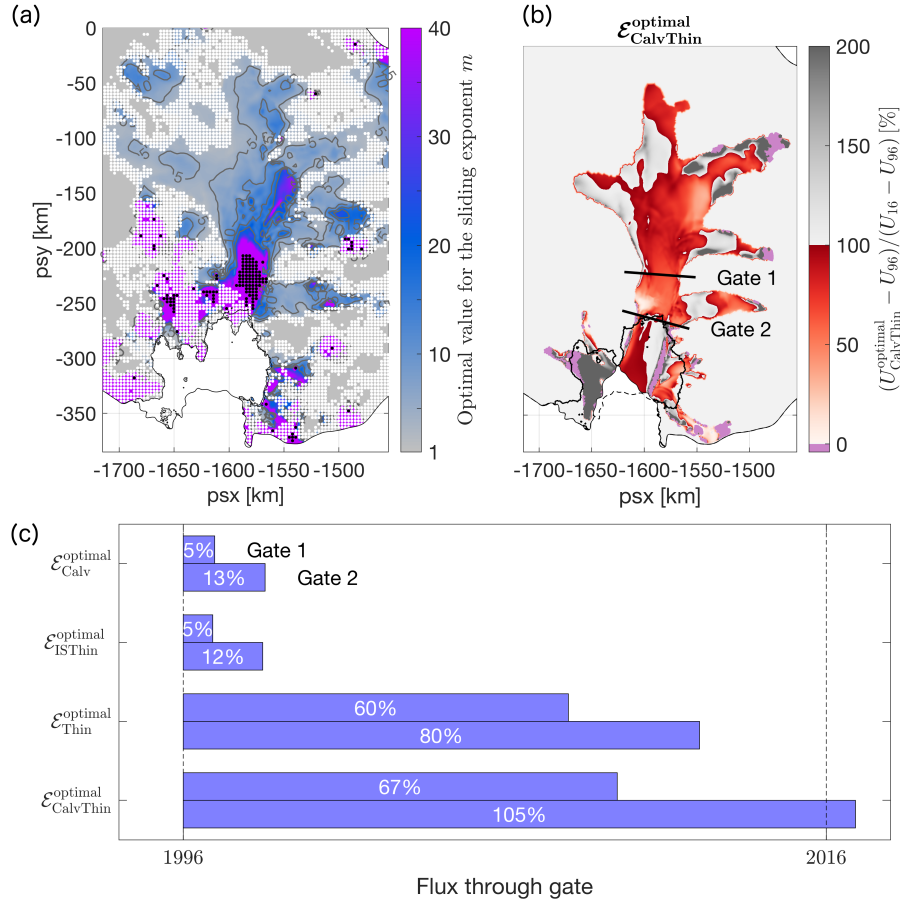


Figure 6. (a) Optimal values of the sliding exponent, required to ensure close agreement between modeled and observed changes in flow velocity of Pine Island Glacier between years 1996 and 2016. White and black dots mark areas where such an agreement cannot be achieved for different reasons: white dots indicate a poor fit between the transfer function $|\mathcal{T}_{US}|$ and $\Delta U_{CalvThin}^{m_i}/\Delta U$, $m_i \in \{1, 3, \dots, 21\}$, with $R^2 < 0.9$; black dots indicate areas where a positive, finite solution for $m_{optimal}$ in Eq. 5 does not exist, and [Weertman non-linear viscous](#) sliding cannot reproduce observed changes in surface flow. (b) Same as Fig. 3d but for optimal values of the sliding law exponent in panel a. (c) Same as Fig. 3e but for optimal values of the sliding law exponent in panel a.

uncertainties, or approaches the limit $\Delta U \rightarrow 0$. In these areas, the non-linear regression was generally found to be poor, with R^2 values smaller than 0.9 as indicated by the white dots in Fig. 6a. As no reliable estimate for $m_{optimal}$ could be obtained for areas shaded in white or black in Fig. 6a, values were instead based on a nearest-neighbour interpolation.

It is important to reiterate that the used regression method crucially relies on non-trivial measurements of changes in surface velocity ($\Delta U \neq 0$), and cannot be used to retrieve information about the basal rheology of ice bodies that are presently in steady state. It should also be noted that values of $f_1(\mathbf{x})$ and $f_2(\mathbf{x})$ were derived independently for each node of the computational mesh, whereas the continuum mechanical properties of glacier flow would suggest a non-zero spatial covariance

415 $\langle f_1(x_1), f_1(x_2) \rangle \neq 0$ and $\langle f_2(x_1), f_2(x_2) \rangle \neq 0$. The optimal solution for m is therefore not automatically mesh independent or robust with respect to the amount of regularization in the inversion. This concern is discussed further in App. D.

In order to demonstrate the improved model response to thinning and calving for a spatially variable sliding exponent $m_{\text{optimal}}(\mathbf{x})$, we performed a new inversion with $m_{\text{optimal}}(\mathbf{x})$, and subsequently repeated the geometric perturbation experiments $\mathcal{E}_*^{\text{optimal}}$. The results are presented in Fig. 6b and c. Compared to spatially uniform values of m (Fig. 3d and Fig. 5),
420 a spatially variable basal rheology generally improves the fit between observed changes in flow and the modeled response across the entire basin. Based on the flux changes through Gate 1 and 2, we find that (1) calving and ice thickness changes in combination with a spatially variable, predominantly plastic bed rheology account for 67% and 105% of flux changes through Gate 1 and 2 respectively, compared to 28% and 64% for a uniform non-linear viscous sliding law with exponent $m = 3$, that (2) calving and ice shelf thinning caused an almost identical response in ice dynamics upstream of the grounding line,
425 and that (3) dynamic thinning and grounding line movement account for most of the flux changes between years 1996 and 2016. The remaining mismatch between the observed and modeled response in Fig. 6b can, at least in part, be attributed to uncertainties in $m_{\text{optimal}}(\mathbf{x})$. This is of particular relevance in the vicinity of the grounding line and for parts of the central trunk, where the non-linear regression method in Eq. 4 did not provide a reliable or finite estimate for m_{optimal} , ~~and where Weertman theory of sliding could break down all together (Iverson et al., 1998; Schoof, 2006).~~ Previous studies, e.g. by Gillet-Chaulet et al. (2016) and Joughin et al. (2019) have demonstrated a better agreement between modeled and observed speed-up using Coulomb-limited sliding laws, such as those proposed by Budd et al. (1984); Schoof (2006); Tsai et al. (2015). Our results are consistent with these earlier studies, and suggest that power-law sliding does not adequately capture the physical relationship between basal shear stress and sliding in the vicinity of the grounding line.

4 Conclusions

435 Based on the most comprehensive observations of ice shelf and grounded ice thickness changes to date, and a suite of diagnostic model experiments with the contemporary flow model Úa, we have analyzed the relative importance of ice shelf thinning, calving and grounding line retreat for the speed-up of Pine Island Glacier between years 1996 and 2016. The detailed comparison between simulated and observed changes in flow speed has provided ~~unprecedented~~ insights into the ability of a modern-day ice flow model to reproduce dynamic changes in response to prescribed geometric perturbations. Significant discrepancies
440 between observed and modeled changes in flow were found, and were addressed by either allowing changes in ice viscosity and basal slipperiness, or by varying the mechanical properties of the ice-bed interface. For non-linear viscous sliding at the bed, geometric perturbations could only account for 64% of the observed flux increases close to the grounding line, whereas the remaining 36% could be attributed to large and widespread changes in ice viscosity (including damage) and/or changes in basal slipperiness. Under the alternative assumption that ice viscosity and basal slipperiness did not change considerably over
445 the last two decades, we found that the recent increase in flow speed of Pine Island Glacier is only compatible with observed patterns of thinning if a heterogeneous, predominantly plastic bed underlies large parts of the central glacier and its upstream tributaries, consistent with earlier findings.

Code and data availability. The open-source ice flow model *Úa* is available from Gudmundsson (2020). All model configurations files specific to this study, as well as model output and plotting routines for each figure are available from DOI TBC. Ice shelf thinning rates are
450 available upon request from FP.

Appendix A: Observations of Pine Island Ice Shelf thickness changes between 1996 and 2016

We derived a new ice-shelf height time series from measurements acquired by four overlapping ESA satellite radar altimetry (RA) missions: ERS-1 (1991–1996), ERS-2 (1995–2003), Envisat (2002–2012), and CryoSat-2 (2010–present). For this study, we constructed a record of ice-shelf height spanning 20 years (1996–2016), with a temporal sampling of 3 months. We
455 integrated all measurements along the satellite ground tracks and gridded the solution on a 3 by 3 km grid.

Our adopted processing steps for RA data are a modification/improvement from Paolo et al. (2016) and Nilsson et al. (2016). Specifically for CryoSat-2, we retracked ESA’s SARIn L1B product over the Antarctic ice shelves using the approach by Nilsson et al. (2016); we corrected for a 60 m range offset for data with surface types ‘land’ or ‘closed sea’; and removed points with anomalous backscatter values (>30 dB). We estimated heights with a modified (from McMillan et al. (2014))
460 surface-fit approach, with a variable rather than constant search radius to account for the RA heterogeneous spatial distribution, and calculating mean values along the satellite reference tracks; we removed height estimates less than 2 m above the Eigen-6C4 geoid (Chuter and Bamber, 2015) to account for ice-shelf mask imperfections near the calving front; applied all of the standard corrections to altimeter data over ice shelves (for example, removed gross outliers, and residual heights with respect to mean topography > 15 m; ran an iterative three-sigma filter; minimized the effect of variations in backscatter (Paolo et al.,
465 2016); corrected for ocean tides (Padman et al., 2002) and inverse barometer effects (Padman et al., 2004).

We then gridded the height data in space and time on a $3\text{ km} \times 3\text{ km} \times 3\text{ month}$ cube, for each mission independently. We merged the records (all four satellites) by only accepting time series that overlapped by at least three quarters of a year to ensure proper cross-calibration, and removed (and subsequently interpolated) anomalous data points that deviated from the trend by more than 5 std. This removes data with, for example, satellite mispointing, anomalous backscatter fluctuations, grounded-ice
470 contamination, high surface slopes and geolocation errors. We fitted linear trends to the gridded product to obtain the ΔH field used in our model experiments (see Sect. 2.1). We also removed a 3 km buffer around the ice-shelf boundaries to further mitigate floating-grounded mask imperfections, and the limitation of geophysical corrections within the ice-shelf flexural zone.

The thickness changes for the ice shelf were combined with existing data for thickness changes over the same time period on the grounded ice (Shepherd et al., 2016). The resulting dataset for ΔH , as used in the experiments described in Sect. 2.2, is shown in Fig. A1. The figure shows the data grids, including the 3 km buffer downstream of the 1996 grounding line, and other data sparse areas along the central flowline. Here, thickness changes were obtained through linear interpolation from neighbouring data. The grounding line location associated with our 1996 thickness distribution was compared to independent measurments from DInSAR (Rignot et al., 2014), and both agree well (Fig.A1).
475

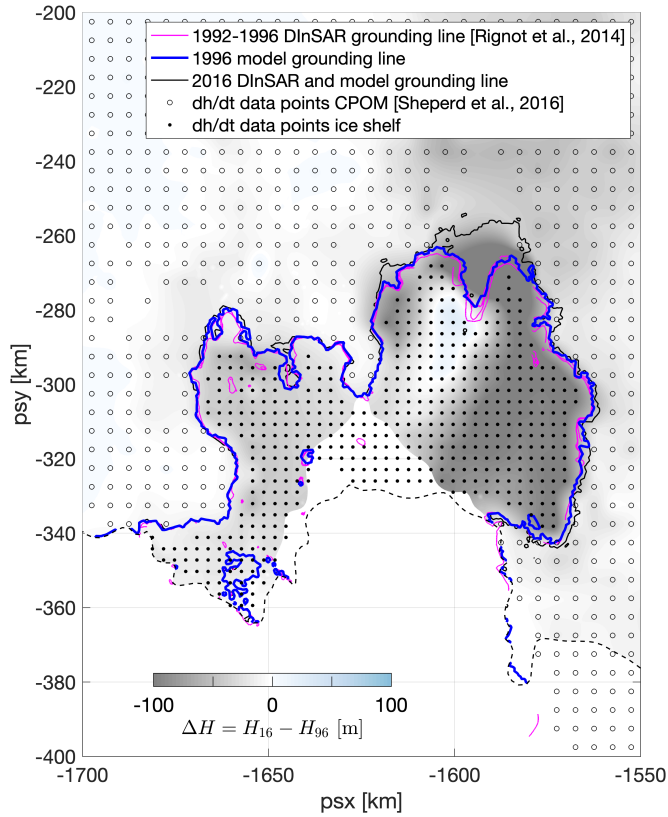


Figure A1. Ice thickness changes (ΔH) between 1996 and 2016, based on a comprehensive analysis of satellite altimeter data. The altimeter data coverage is represented by dots (ice shelf) and circles (grounded ice, (Shepherd et al., 2016)). The final 1996 ice thickness distribution was obtained by subtracting ΔH from the 2016 Bedmachine ice thickness (Morlighem et al., 2020), as described in Sect.2.1. The associated 1996 grounding line location (blue line) compares well to independent DInSAR measurements (magenta line, (Rignot et al., 2014)).

Appendix B: Model configuration and inverse methodology

480 The open source ice flow model $\dot{U}a$ (Gudmundsson, 2020) uses finite element [methods-method](#) to solve the shallow ice stream equations, commonly referred to as SSA or SSTREAM ([Hutter, 1983](#); [MacAyeal, 1989](#)), on an irregular triangular mesh. The diagnostic velocity solver is based on an iterative Newton-Raphson method. A fixed mesh with 109,300 linear elements was used with a median nodal spacing of 1.2 km and local mesh refinement down to 500 m in areas with above-average horizontal shear, strong gradients in ice thickness and within a 10 km buffer around the grounding line. The mesh was generated using the

485 open-source generator mesh2d (Engwirda, 2014).

The [inverse optimization](#) capabilities of $\dot{U}a$ follow commonly applied techniques in ice flow modeling to optimize uncertain model parameters, p_i , based on prior information, \hat{p}_i , and a range of observations with associated measurement errors ([MacAyeal, 1992](#)). $\dot{U}a$ uses an adjoint method to obtain a combined optimal estimate of the spatially varying rate factor A and

basal slipperiness C across the full model domain, for given observations of surface velocity u_{obs} and measurement errors ε_u .
 490 Optimal values for $p_i \in \{A, C\}$ were obtained as a solution to the minimization problem $d_p J$ with the cost function J defined as the sum of the misfit term I and Tikhonov regularization R : $J = I + R$, with

$$I = \frac{1}{2\mathcal{A}} \int dx (u_{\text{model}} - u_{\text{obs}})^2 / \varepsilon_u^2, \quad (\text{B1})$$

$$R = \frac{1}{2\mathcal{A}} \int dx \sum_i \left(\gamma_{s,i,s}^2 (\nabla \log_{10}(p_i / \hat{p}_i))^2 + \gamma_{i,a}^2 (\log_{10}(p_i / \hat{p}_i))^2 \right), \quad (\text{B2})$$

and $\mathcal{A} = \int dx$ the total area of the model domain. ~~A Spatially constant a priori values of the rate factor and slipperiness~~
 495 were chosen as $\hat{A} = 5.04 \times 10^{-9} \text{ kPa}^{-3} \text{ yr}^{-1}$, which corresponds to a spatially uniform ice temperature of -15°C (Cuffey and Paterson, 2010), and $\hat{C} = u_b \tau^{-m}$, with $u_b = 750 \text{ m yr}^{-1}$ and $\tau = 80 \text{ kPa}$ and m the sliding law exponent. An iterative interior point optimization algorithm was used to calculate $d_p J$ and stopped after 10^4 iterations, when fractional changes to the cost function were less than 10^{-5} . ~~An optimal value for the Tikhonov regularization multiplier, γ_s , in the cost function was~~

~~The gradient and amplitude contributions in the regularization term (R in Eq.B1) are multiplied by spatially-constant~~
 500 ~~Tikhonov regularization multipliers, $\gamma_{i,s}$ and $\gamma_{i,a}$. Optimal values for $\gamma_{i,s}$ and $\gamma_{i,a}$ were~~ determined using an L-curve approach, ~~as. For $\gamma_{i,s}$ results are~~ shown in Fig. B1. The ~~value-values $\gamma_s = 25000$ $\gamma_{A,s} = \gamma_{C,s} = 25000$ m~~ was used for all experiments in the main part of the text, as it produced the smallest misfit between observed and modelled surface velocities whilst limiting the risk of overfitting. The sensitivity of the main results with respect to the choice of γ_s is discussed in App. D. ~~A similar L-curve approach was followed to determine an optimal values for $\gamma_{i,a}$, and $\gamma_{A,a} = \gamma_{C,a} = 1$ was used throughout this study.~~

505 Figure B1 shows the difference between u_{model} and u_{obs} (panel **b**), and corresponding optimal estimates of A (panel **c**) and C (panel **d**) for $\gamma_s = 25000 \text{ m}$. Modeled surface velocities are typically within 30 meters per year or less of the observed values, with a mean misfit of -1.68 m yr^{-1} and standard deviation of 15.3 m yr^{-1} . The highest values of the rate factor are generally found within the shear margins, with positive equivalent ice temperatures suggesting the presence of a complex rheology or damage. The highest values of the slipperiness are consistently found in the fast-flowing central part of the glacier and along
 510 its upstream tributaries, with noticeably reduced values of C in an area between 5 and 40 km upstream of the 1996 grounding line. These results are broadly in agreement with previously published maps, see e.g. Arthern et al. (2015).

Appendix C: Non-linear dependency of the flow response on the sliding exponent

The transfer amplitude $|\mathcal{T}_{US}|$, defined in Eq. 4, describes the linear response of the along-slope surface velocity to small harmonic perturbations in the surface elevation or, equivalently, ice thickness. Analytical solutions for the transfer function
 515 \mathcal{T}_{US} (amplitude and phase) in the framework of the shallow ice stream approximation with a linear ice rheology ($n = 1$ in Eq. 2) and a non-linear viscous ~~Weertman sliding-sliding law~~ (arbitrary m in Eq. 3) were previously obtained by Gudmundsson (2008). Note that the original expression (Eq. 29 in Gudmundsson (2008)) contained a printing error so we repeat the correct form here:

$$\mathcal{T}_{US} = \frac{\tau_d [m\gamma(1 + \psi) + \eta H (j^2 \psi + k^2 + 4l^2)]}{Hm\gamma^2 + \gamma\eta H^2 [l^2(4 + m) + k^2(1 + 4m)] + 4H^3 j^4 \eta^2}, \quad (\text{C1})$$

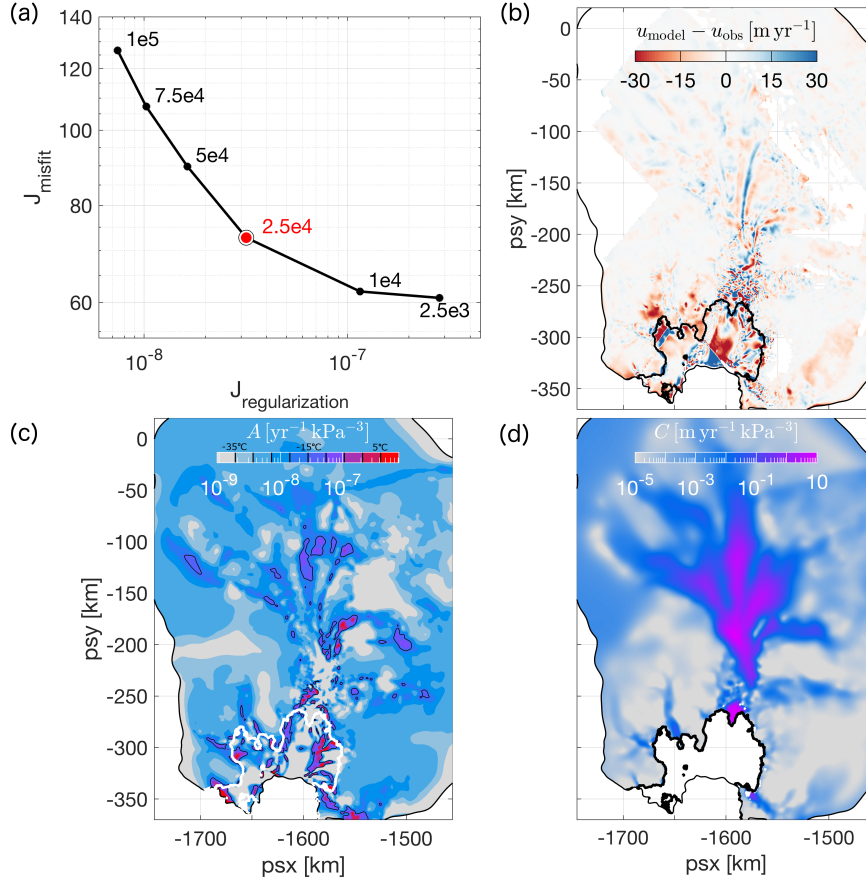


Figure B1. (a) L-curve used to determine the optimal value of the Tikhonov regularization multiplier γ_s , highlighted in red. (b) Misfit between modeled and observed surface speed in 1996 for $\gamma_s = 25000\text{m}$. (c) Rate factor (A in Eq. 2) in 1996, obtained as a minimum of the cost function J in Eq. B1 with $\gamma_s = 25000\text{m}$. The equivalent depth-averaged ice temperature ranges from $-35\text{ }^\circ\text{C}$ (grey) to $5\text{ }^\circ\text{C}$ (red). Colors are discretized at $5\text{ }^\circ\text{C}$ intervals and the black lines indicate the $0\text{ }^\circ\text{C}$ contour. The white line corresponds to the 1996 grounding line position. (d) Optimal value of the basal slipperiness (C in Eq. 3) in 1996, estimated using the adjoint minimization approach.

520 where H is the local ice thickness, α is the local bed slope, ρ is the ice viscosity, $\tau_d = \rho g H \sin \alpha$ is the driving stress, η is the effective viscosity and $\gamma = \frac{\tau_d^{1-m}}{mC}$, $\psi = ikH \cot \alpha$ and $j^2 = k^2 + l^2$ are abbreviations, with k and l the along-slope and transverse wavelength respectively of the harmonic surface perturbation. Since we focus on the instantaneous response of the velocity to perturbations at the surface, the exponential decay of \mathcal{T}_{US} with time has been omitted. An equivalent expression for the response of the transverse velocity component can be derived; we refer to Gudmundsson (2008) for more details.

525 Following Gudmundsson (2008), physical quantities can be rescaled to obtain the non-dimensional form of the transfer function. After substitution of the scalings $H \rightarrow 1$, $\eta \rightarrow 1/2$, $\tau_d \rightarrow 1$ into Eq. C1 and some reordering, one obtains

$$\mathcal{T}_{US} = \frac{m \left[\frac{1}{C} (1 + \psi) + \frac{1}{2} (j^2 \psi + k^2 + 4l^2) \right]}{m \left[j^4 + \frac{1}{2C} (l^2 + 4k^2) \right] + \frac{1}{C^2} + \frac{1}{2C} (4l^2 + k^2)}. \quad (\text{C2})$$

The resulting transfer amplitude takes the form $|\mathcal{T}_{US}| = \frac{f_1 m}{m + f_2}$ as in Eq. 4, where functions f_1 and f_2 depend on C , α , k and l .

530 The analytical expression in Eq. C2 describes the first-order response to small perturbations in ice thickness, $\delta H \ll 1$, for well-defined length scales characterized by k and l . However, in a realistic setting such as PIG, the system responds to a complicated perturbation composed of a range of wavelengths and amplitudes, and Eq. C2 does not automatically hold. Based on experiments $\mathcal{E}_{\text{CalvThin}}^{m_i}$, $m_i \in \{1, 3, \dots, 21\}$ presented in Sect. 3.3, we found that the simulated surface response of PIG to observed geometrical perturbations retains its dependency on m of the form $\frac{f_1 m}{m + f_2}$, but more complicated expressions for f_1 and f_2 are required that do not exist in analytical form. A best-estimate for the spatially varying fields f_1 and f_2 was obtained by
 535 minimizing the misfit between $\Delta U_{\text{CalvThin}}^{m_i} / \Delta U$, $m_i \in \{1, 3, \dots, 21\}$ and $\frac{f_1 m}{m + f_2}$. The resulting misfit, quantified by R^2 values, is summarized in Fig. C1a. Red and black areas indicate a good fit with $R^2 \geq 0.9$, though an important distinction was made between solutions with $f_1 \geq 100$ (red) and $f_1 < 100$ (black). The difference between both cases is explained further in Sect. 3.3. Examples of the fit at locations 1 and 2 are shown in Fig. C1b and c respectively. Grey shading in Fig. C1a corresponds to a poor fit ($R^2 < 0.9$) and the dependency of $\Delta U_{\text{CalvThin}}^m / \Delta U$ on m cannot be adequately described by the function $\frac{f_1 m}{m + f_2}$.
 540 Possible reasons for this discrepancy are discussed in Sect. 3.3.

Appendix D: Dependency of the results on the regularization

The inverse problem of inferring information about the rate factor A and basal slipperiness C from uncertain observations of surface velocity is generally ill-posed. To remedy the ill-posedness of the problem, additional information in the form of a regularization term (Eq. B2) is commonly added to the cost function. ~~In a Bayesian framework, the regularization plays the role of a prior and is added to the misfit, which corresponds to the likelihood.~~
 545 The solution of the minimization problem generally depends on the choice of regularization. In the specific case of a Tikhonov regularization, which is used throughout this study, the solution for A and C will depend on the unknown ~~multiplier γ_s~~ multipliers $\gamma_{i,a}$ and $\gamma_{i,s}$, and the choice of prior information $\hat{\rho}_i$ in Eq. B2. One method to choose an ‘optimal’ value for ~~γ_s~~ the multipliers is the L-curve approach presented in App. B. However, this is an ad-hoc method and it remains to be shown that results are robust for a range of ~~γ_s values.~~ γ values. ~~Below~~
 550 we discuss the robustness of our results for a range γ_s values. A similar analysis was carried out for a range of γ_a values and priors, but those results did not affect our conclusions and are not shown here.

In case of the perturbation experiments \mathcal{E}_*^3 , which were designed to simulate the velocity response to a series of prescribed changes in the PIG geometry, we are primarily interested in the γ_s -dependency of the relative fluxes in Fig. 3e. In addition to the experiments with default value $\gamma_s = 25000\text{m}$, identical perturbation experiments were carried out for $\gamma_s = 10000\text{m}$ and
 555 $\gamma_s = 50000\text{m}$. The corresponding changes in flux, presented in Table D1, do not show any significant variability with γ_s and results presented in Sect. 3.1 can be considered robust, at least across the range of tested γ_s values.

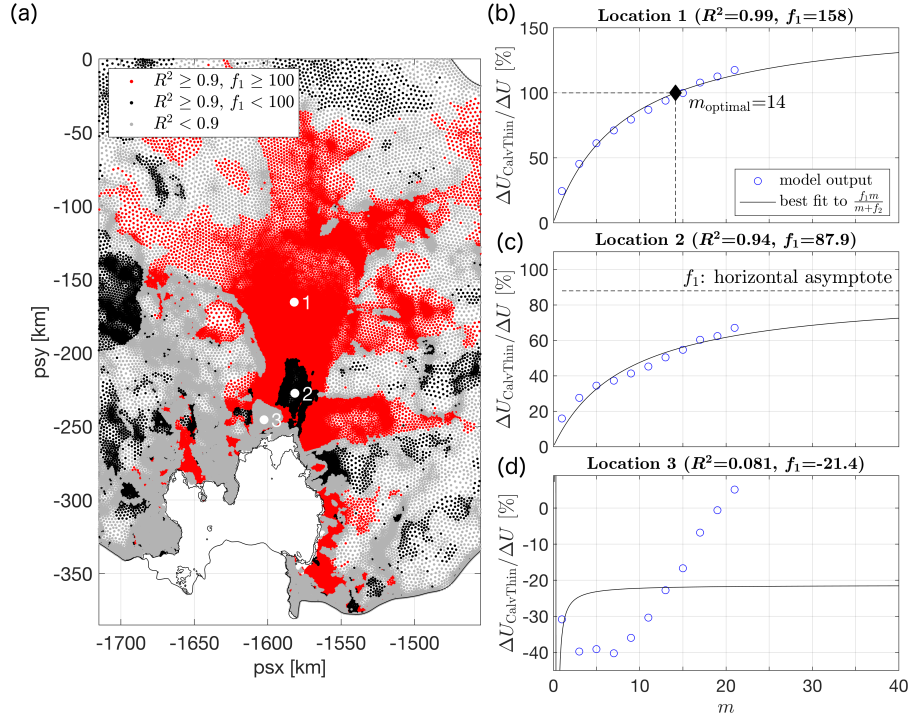


Figure C1. (a) Goodness of fit between $\frac{f_1 m}{m+f_2}$ and model simulations $\Delta U_{\text{CalvThin}}^{m_i}/\Delta U$, $m_i \in \{1, 3, \dots, 21\}$. Red areas correspond to $R^2 \geq 0.9$ and fitting parameter $f_1 \geq 100$. An example of the fit at location 1 and resulting m_{optimal} (Eq. 5) are shown in panel b. Black areas in (a) correspond to $R^2 \geq 0.9$ and fitting parameter $f_1 < 100$. The horizontal asymptote with limit < 100 indicates that a positive, finite solution m_{optimal} does not exist, and Weertman sliding cannot reproduce 100% of the observed changes in surface velocity. An example of the fit and asymptote at location 2 are shown in panel c. Grey areas in (a) correspond to $R^2 < 0.9$, indicating a poor fit between $\frac{f_1 m}{m+f_2}$ and $\Delta U_{\text{CalvThin}}^{m_i}/\Delta U$, $m_i \in \{1, 3, \dots, 21\}$. An example at location 3 is shown in panel d.

Experiments \mathcal{E}_A^3 and \mathcal{E}_C^3 were also repeated for $\gamma_s = 10000\text{m}$ and $\gamma_s = 50000\text{m}$. Maps of A and C (not shown) were compared to the default results for $\gamma_s = 25000\text{m}$ shown in Fig. 4, and no significant qualitative differences were found.

Perturbation experiments \mathcal{E}_*^m for a range of sliding law exponents $1 \leq m \leq 21$ were repeated for $\gamma_s = 10000\text{m}$ and $\gamma_s = 50000\text{m}$. Following the approach outlined in Sect. 3.3, an optimal spatial distribution of the sliding exponent was computed for each γ_s . Results are presented in Fig. D1 and show a decreasing trend in m_{optimal} for increasing values of the regularization multiplier γ_s . In particular, the area where no positive, finite solution exist for m_{optimal} (shaded in black) is reduced in size and eventually disappears for increasing amounts of regularization. However, the spatial distribution of m_{optimal} is found to be in broad agreement across the considered range of γ_s .

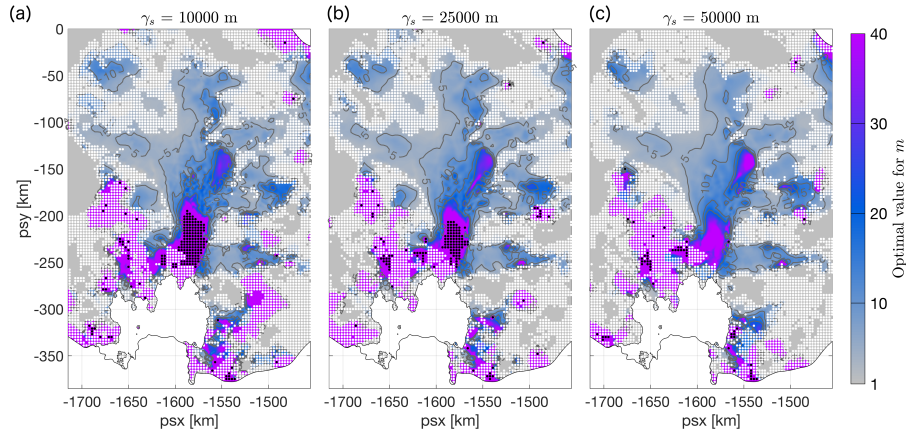


Figure D1. Optimal distribution of m , as in Fig. 6a, for different values of the regularization multiplier: (a) $\gamma_s = 10000$ m, (b) $\gamma_s = 25000$ m and (c) $\gamma_s = 50000$ m. White dots indicate areas where results for the non-linear regression method were poor, with a R^2 -value smaller than 0.9. Black dots indicate areas where the value of f_1 in the fit is less than 100, indicating that agreement between simulated and observed changes in surface velocity cannot be achieved for finite values of m . The value $\gamma_s = 25000$ m was used throughout the main part of this study.

Table D1. Sensitivity of the relative flux changes in the \mathcal{E}_*^3 experiments (see Fig. 3) with respect to the choice of regularization multiplier γ_s . The optimal value, $\gamma_s = 25000$ m, used throughout this study was based on the L-curve presented in Fig. B1.

		$\gamma_s = 10000$ m	$\gamma_s = 25000$ m	$\gamma_s = 50000$ m
$\mathcal{E}_{\text{Calv}}^3$	Gate 1	2%	2%	2%
	Gate 2	15%	13%	13%
$\mathcal{E}_{\text{ISThin}}^3$	Gate 1	2%	2%	2%
	Gate 2	14%	13%	12%
$\mathcal{E}_{\text{Thin}}^3$	Gate 1	24%	26%	25%
	Gate 2	38%	45%	42%
$\mathcal{E}_{\text{CalvThin}}^3$	Gate 1	26%	28%	27%
	Gate 2	58%	64%	58%

565 *Author contributions.* JDR and RR designed and initiated the project and prepared the manuscript; FP processed the ice shelf thickness data; JDR performed the model simulations, carried out the analysis and produced the figures; FP and GHG reviewed and edited the paper.

Competing interests. JDR serves as topical editor for The Cryosphere.

Acknowledgements. JDR, GHG and RR are supported by the TiPACCs project that receives funding from the European Union's Horizon 2020 research and innovation programme under grant agreement no. 820575. RR is further supported by the Deutsche Forschungsgemeinschaft (DFG) by grant WI4556/3-1 and GHG by the NSFPLR-NERC grant: *Processes, drivers, predictions: Modelling the response of Thwaites Glacier over the next century using ice/ocean coupled models* (NE/S006745/1).

References

- Alley, K. E., Scambos, T. A., Alley, R. B., and Holschuh, N.: Troughs developed in ice-stream shear margins precondition ice shelves for ocean-driven breakup, *Science Advances*, 5, 1–8, <https://doi.org/10.1126/sciadv.aax2215>, 2019.
- 575 Arndt, J. E., Larter, R. D., Friedl, P., Gohl, K., Höppner, K., et al.: Bathymetric controls on calving processes at Pine Island Glacier, *The Cryosphere*, 12, 2039–2050, 2018.
- Arthern, R. J. and Williams, C. R.: The sensitivity of West Antarctica to the submarine melting feedback, *Geophysical Research Letters*, 44, 2352–2359, <https://doi.org/10.1002/2017GL072514>, 2017.
- Arthern, R. J., Hindmarsh, R. C., and Williams, C. R.: Flow speed within the Antarctic ice sheet and its controls inferred from satellite
580 observations, *Journal of Geophysical Research F: Earth Surface*, 120, 1171–1188, <https://doi.org/10.1002/2014JF003239>, 2015.
- Bamber, J. L. and Dawson, G. J.: Complex evolving patterns of mass loss from Antarctica’s largest glacier, *Nature Geoscience*, pp. 1–5, 2020.
- Brondeix, J., Gillet-Chaulet, F., and Gagliardini, O.: Sensitivity of centennial mass loss projections of the Amundsen basin to the friction law, *The Cryosphere*, 13, 177–195, 2019.
- 585 Budd, W. F., Janssen, D., and Smith, I. N.: A Three-Dimensional Time-Dependent Model of the West Antarctic Ice Sheet, *Annals of Glaciology*, 5, 29–36, <https://doi.org/10.3189/1984AoG5-1-29-36>, 1984.
- Christianson, K., Bushuk, M., Dutrieux, P., Parizek, B. R., Joughin, I. R., Alley, R. B., Shean, D. E., Abrahamsen, E. P., Anandakrishnan, S., Heywood, K. J., Kim, T.-W., Lee, S. H., Nicholls, K., Stanton, T., Truffer, M., Webber, B. G. M., Jenkins, A., Jacobs, S., Bindschadler, R., and Holland, D. M.: Sensitivity of Pine Island Glacier to observed ocean forcing, *Geophysical Research Letters*, 43, 10,817–10,825,
590 <https://doi.org/10.1002/2016GL070500>, 2016.
- Chuter, S. J. and Bamber, J. L.: Antarctic ice shelf thickness from CryoSat-2 radar altimetry, *Geophysical Research Letters*, 42, 10721–10729, <https://doi.org/10.1002/2015GL066515>, 2015.
- Cuffey, K. and Paterson, W.: *The physics of glaciers*, 4th Edition, [https://doi.org/10.1016/0016-7185\(71\)90086-8](https://doi.org/10.1016/0016-7185(71)90086-8), 2010.
- Dutrieux, P., De Rydt, J., Jenkins, A., Holland, P. R., Ha, H. K., Lee, S. H., Steig, E. J., Ding, Q., Abrahamsen, E. P., and Schröder, M.:
595 Strong sensitivity of Pine Island ice-shelf melting to climatic variability, *Science*, 343, 174–178, 2014.
- Engwirda, D.: *Locally-optimal Delaunay-refinement and optimisation-based mesh generation*, Ph.D. thesis, The University of Sydney, <http://hdl.handle.net/2123/13148>, 2014.
- Favier, L., Durand, G., Cornford, S., Gudmundsson, G., Gagliardini, O., Gillet-Chaulet, F., Zwinger, T., Payne, A., and Brocq, A.: Retreat of Pine Island Glacier controlled by marine ice-sheet instability, *Nature Clim. Change*, advance online publication,
600 <https://doi.org/10.1038/nclimate2094>, 2014.
- Gardner, A. S., Moholdt, G., Scambos, T., Fahnestock, M., Ligtenberg, S., Van Den Broeke, M., and Nilsson, J.: Increased West Antarctic and unchanged East Antarctic ice discharge over the last 7 years, *Cryosphere*, 12, 521–547, <https://doi.org/10.5194/tc-12-521-2018>, 2018.
- Gillet-Chaulet, F., Durand, G., Gagliardini, O., Mosbeux, C., Mouginot, J., Rémy, F., and Ritz, C.: Assimilation of surface velocities acquired between 1996 and 2010 to constrain the form of the basal friction law under Pine Island Glacier, *Geophysical Research Letters*, 43, 10–311,
605 2016.
- Gudmundsson, G. H.: Analytical solutions for the surface response to small amplitude perturbations in boundary data in the shallow-ice-stream approximation, *The Cryosphere*, 2, 77–93, <https://doi.org/10.5194/tc-2-77-2008>, 2008.
- Gudmundsson, G. H.: GHilmarG/UaSource: Ua2019b (Version v2019b), <http://doi.org/10.5281/zenodo.3706623>, 2020.

- Gudmundsson, G. H., Krug, J., Durand, G., Favier, L., and Gagliardini, O.: The stability of grounding lines on retrograde slopes, *Cryosphere*, 6, 1497–1505, <https://doi.org/10.5194/tc-6-1497-2012>, 2012.
- 610 Gudmundsson, G. H., Paolo, F. S., Adusumilli, S., and Fricker, H. A.: Instantaneous Antarctic ice sheet mass loss driven by thinning ice shelves, *Geophysical Research Letters*, 46, 13 903–13 909, <https://doi.org/10.1029/2019GL085027>, 2019.
- Howat, I. M., Porter, C., Smith, B. E., Noh, M.-J., and Morin, P.: The Reference Elevation Model of Antarctica, *The Cryosphere*, 13, 665–674, <https://doi.org/10.5194/tc-13-665-2019>, <https://www.the-cryosphere.net/13/665/2019/>, 2019.
- 615 Hutter, K.: *Theoretical Glaciology: Material Science of Ice and the Mechanics of Glaciers and Ice Sheets*, Mathematical Approaches to Geophysics, Springer, 1983.
- Iverson, N., Hooyer, T., and Baker, R.: Ring-shear studies of till deformation: Coulomb-plastic behavior and distributed strain in glacier beds, *Journal of Glaciology*, 44, 634–642, <https://doi.org/10.3189/s0022143000002136>, 1998.
- Jenkins, A., Dutrieux, P., Jacobs, S., Mcphail, S., Perrett, J., Webb, A., and White, D.: Observations beneath Pine Island Glacier in West Antarctica and implications for its retreat, *Nature Geoscience*, 3, 468–472, <https://doi.org/10.1038/ngeo890>, 2010.
- 620 Jenkins, A., Dutrieux, P., Jacobs, S., Steig, E., Gudmundsson, G., Smith, J., and Heywood, K.: Decadal Ocean Forcing and Antarctic Ice Sheet Response: Lessons from the Amundsen Sea, *Oceanography*, 29, 106–117, <https://doi.org/10.5670/oceanog.2016.103>, 2016.
- Joughin, I., Tulaczyk, S., Bamber, J. L., Blankenship, D., Holt, J. W., Scambos, T., and Vaughan, D. G.: Basal conditions for Pine Island and Thwaites Glaciers, West Antarctica, determined using satellite and airborne data, *Journal of Glaciology*, 55, 245–257, <https://doi.org/10.3189/002214309788608705>, 2009.
- 625 Joughin, I., Smith, B. E., and Holland, D. M.: Sensitivity of 21st century sea level to ocean-induced thinning of Pine Island Glacier, Antarctica, *Geophysical Research Letters*, 37, <https://doi.org/10.1029/2010GL044819>, 2010.
- Joughin, I., Smith, B. E., and Schoof, C. G.: Regularized Coulomb friction laws for ice sheet sliding: application to Pine Island Glacier, Antarctica, *Geophysical research letters*, 46, 4764–4771, 2019.
- 630 Khazendar, A., Rignot, E., and Larour, E.: Larsen B Ice Shelf rheology preceding its disintegration inferred by a control method, *Geophysical Research Letters*, 34, 1–6, <https://doi.org/10.1029/2007GL030980>, 2007.
- Lhermitte, S., Sun, S., Shuman, C., Wouters, B., Pattyn, F., Wuite, J., Berthier, E., and Nagler, T.: Damage accelerates ice shelf instability and mass loss in Amundsen Sea Embayment, *Proceedings of the National Academy of Sciences*, 117, 24 735–24 741, <https://doi.org/10.1073/pnas.1912890117>, 2020.
- 635 MacAyeal, D. R.: Large-scale ice flow over a viscous basal sediment: Theory and application to ice stream B, Antarctica, *Journal of Geophysical Research: Solid Earth*, 94, 4071–4087, <https://doi.org/10.1029/JB094iB04p04071>, 1989.
- MacAyeal, D. R.: The basal stress distribution of ice stream E, Antarctica, inferred by control methods, *Journal of Geophysical Research*, <https://doi.org/10.1029/91JB02454>, 1992.
- McMillan, M., Shepherd, A., Sundal, A., Briggs, K., Muir, A., Ridout, A., Hogg, A., and Wingham, D.: Increased ice losses from Antarctica detected by CryoSat-2, *Geophysical Research Letters*, 41, 3899–3905, <https://doi.org/10.1002/2014GL060111>, 2014.
- 640 Minchew, B., Simons, M., Björnsson, H., Pálsson, F., Morlighem, M., Seroussi, H., Larour, E., and Hensley, S.: Plastic bed beneath Hofsjökull Ice Cap, central Iceland, and the sensitivity of ice flow to surface meltwater flux, *Journal of Glaciology*, 62, 147–158, <https://doi.org/10.1017/jog.2016.26>, 2016.
- Morlighem, M., Rignot, E., Binder, T., Blankenship, D., Drews, R., Eagles, G., Eisen, O., Ferraccioli, F., Forsberg, R., Fretwell, P., Goel, V., Greenbaum, J. S., Gudmundsson, H., Guo, J., Helm, V., Hofstede, C., Howat, I., Humbert, A., Jokat, W., Karlsson, N. B., Lee, W. S., Matsuoka, K., Millan, R., Mouginot, J., Paden, J., Pattyn, F., Roberts, J., Rosier, S., Ruppel, A., Seroussi, H., Smith, E. C.,

- Steinhage, D., Sun, B., den Broeke, M. R., Ommen, T. D., van Wessem, M., and Young, D. A.: Deep glacial troughs and stabilizing ridges unveiled beneath the margins of the Antarctic ice sheet, *Nature Geoscience*, 13, 132–137, <https://doi.org/10.1038/s41561-019-0510-8>, <http://dx.doi.org/10.1038/s41561-019-0510-8>, 2020.
- 650 Mouginit, J., Rignot, E., and Scheuchl, B.: Sustained increase in ice discharge from the Amundsen Sea Embayment, West Antarctica, from 1973 to 2013, *Geophysical Research Letters*, 41, 1576–1584, 2014.
- Mouginit, J., Rignot, E., and Scheuchl, B.: MEASUREs Phase-Based Antarctica Ice Velocity Map, Version 1., <https://doi.org/https://doi.org/10.5067/PZ3NJ5RXRH10>, last accessed 10/2019, 2019a.
- Mouginit, J., Rignot, E., and Scheuchl, B.: Continent-Wide, Interferometric SAR Phase, Mapping of Antarctic Ice Velocity, *Geophysical*
655 *Research Letters*, 46, 9710–9718, <https://doi.org/10.1029/2019GL083826>, 2019b.
- Nilsson, J., Gardner, A., Sørensen, L. S., and Forsberg, R.: Improved retrieval of land ice topography from CryoSat-2 data and its impact for volume-change estimation of the Greenland Ice Sheet, *Cryosphere*, 10, 2953–2969, <https://doi.org/10.5194/tc-10-2953-2016>, 2016.
- Padman, L., Fricker, H. A., Coleman, R., Howard, S., and Erofeeva, L.: A new tide model for the Antarctic ice shelves and seas, *Annals of Glaciology*, 34, 247–254, <https://doi.org/10.3189/172756402781817752>, 2002.
- 660 Padman, L., King, M., Goring, D., Corr, H., and Coleman, R.: Ice-shelf elevation changes due to atmospheric pressure variations, *Journal of Glaciology*, 49, 521–526, <https://doi.org/10.3189/172756503781830386>, 2004.
- Paolo, F., Padman, L., Fricker, H., Adusumilli, S., Howard, S., and Siegfried, M.: Response of Pacific-sector Antarctic ice shelves to the El Niño/Southern Oscillation, *Nature Geoscience*, 1, <https://doi.org/10.1038/s41561-017-0033-0>, 2018.
- Paolo, F. S., Fricker, H. A., and Padman, L.: Constructing improved decadal records of Antarctic ice shelf height change from multiple
665 satellite radar altimeters, *Remote Sensing of Environment*, 177, 192–205, <https://doi.org/10.1016/j.rse.2016.01.026>, 2016.
- Payne, A. J., Vieli, A., Shepherd, A. P., Wingham, D. J., and Rignot, E.: Recent dramatic thinning of largest West Antarctic ice stream triggered by oceans, *Geophysical Research Letters*, 31, 1–4, <https://doi.org/10.1029/2004GL021284>, 2004.
- Pritchard, H., Arthern, R., Vaughan, D., and Edwards, L.: Extensive dynamic thinning on the margins of the Greenland and Antarctic Ice Sheets, *Nature*, 461, 971–5, <https://doi.org/10.1038/nature08471>, 2009.
- 670 Pritchard, H., Ligtenberg, S., Fricker, H., Vaughan, D., Van den Broeke, M., and Padman, L.: Antarctic ice-sheet loss driven by basal melting of ice shelves, *Nature*, 484, 502–5, <https://doi.org/10.1038/nature10968>, 2012.
- Reese, R., Gudmundsson, G. H., Levermann, A., and Winkelmann, R.: The far reach of ice-shelf thinning in Antarctica, *Nature Climate Change*, 8, 53–57, <https://doi.org/10.1038/s41558-017-0020-x>, <http://dx.doi.org/10.1038/s41558-017-0020-x>, 2018.
- Rignot, E.: Changes in West Antarctic ice stream dynamics observed with ALOS PALSAR data, *Geophysical Research Letters*, 35,
675 <https://doi.org/10.1029/2008GL033365>, 2008.
- Rignot, E., Vaughan, D. G., Schmelz, M., Dupont, T., and Macayeal, D.: Acceleration of Pine Island and Thwaites Glaciers, West Antarctica, *Annals of Glaciology*, 34, 189–194, <https://doi.org/10.3189/172756402781817950>, 2002.
- Rignot, E., Mouginit, J., and Scheuchl, B.: Ice Flow of the Antarctic Ice Sheet, *Science*, 333, 1427–1430, <https://doi.org/10.1126/science.1208336>, <https://www.sciencemag.org/lookup/doi/10.1126/science.1208336>, 2011.
- 680 Rignot, E., Mouginit, J., Morlighem, M., Seroussi, H., and Scheuchl, B.: Widespread, rapid grounding line retreat of Pine Island, Thwaites, Smith, and Kohler glaciers, West Antarctica, from 1992 to 2011, *Geophysical Research Letters*, 41, 3502–3509, 2014.
- Rosier, S., Reese, R., Donges, J., De Rydt, J., Gudmundsson, G., and Winkelmann, R.: The tipping points and early-warning indicators for Pine Island Glacier, West Antarctica, <https://doi.org/10.31223/osf.io/y95r6>, 2020.

- Schmeltz, M., Rignot, E., Dupont, T. K., and Macayeal, D. R.: Sensitivity of Pine Island Glacier, West Antarctica, to changes in ice-shelf and basal conditions: A model study, *Journal of Glaciology*, 48, 552–558, <https://doi.org/10.3189/172756502781831061>, 2002.
- Schoof, C.: Variational methods for glacier flow over plastic till, *Journal of Fluid Mechanics*, 555, 299–320, <https://doi.org/10.1017/S0022112006009104>, 2006.
- Seroussi, H., Morlighem, M., Rignot, E., Mouginot, J., Larour, E., Schodlok, M., and Khazendar, A.: Sensitivity of the dynamics of Pine Island Glacier, West Antarctica, to climate forcing for the next 50 years, *Cryosphere*, 8, 1699–1710, <https://doi.org/10.5194/tc-8-1699-2014>, 2014.
- Shepherd, A., Wingham, D., Mansley, J., and Corr, H.: Inland Thinning of Pine Island Glacier, West Antarctica, *Science (New York, N.Y.)*, 291, 862–4, <https://doi.org/10.1126/science.291.5505.862>, 2001.
- Shepherd, A., Wingham, D., and Rignot, E.: Warm ocean is eroding West Antarctic ice sheet. *Geophys Res Lett* 31(L23):402, *Geophysical Research Letters*, 31, <https://doi.org/10.1029/2004GL021106>, 2004.
- Shepherd, A., Hogg, A., Muir, A., and McMillan, M.: Surface Elevation Changes of the Antarctic Ice Sheet from Satellite Radar Altimetry, Antarctic-CCI-SEC-v1.0, 2016.
- Smith, J. A., Andersen, T. J., Shortt, M., Gaffney, A., Truffer, M., Stanton, T., Bindschadler, R., Dutrieux, P., Jenkins, A., Hillenbrand, C.-D., et al.: Sub-ice-shelf sediments record history of twentieth-century retreat of Pine Island Glacier, *Nature*, 541, 77–80, 2017.
- Steig, E., Ding, Q., Battisti, D., and Jenkins, A.: Tropical forcing of Circumpolar Deep Water Inflow and outlet glacier thinning in the Amundsen Sea Embayment, West Antarctica, *Annals of Glaciology*, 53, 19–28, <https://doi.org/10.3189/2012AoG60A110>, 2012.
- Sun, S., Cornford, S. L., Moore, J. C., Gladstone, R., and Zhao, L.: Ice shelf fracture parameterization in an ice sheet model, *Cryosphere*, 11, 2543–2554, <https://doi.org/10.5194/tc-11-2543-2017>, 2017.
- Tsai, V. C., Stewart, A. L., and Thompson, A. F.: Marine ice-sheet profiles and stability under Coulomb basal conditions, *Journal of Glaciology*, 61, 205–215, <https://doi.org/10.3189/2015JoG14J221>, 2015.
- Tulaczyk, S., Kamb, W. B., and Engelhardt, H. F.: Basal mechanics of Ice Stream B, west Antarctica: 1. Till mechanics, *Journal of Geophysical Research: Solid Earth*, 105, 463–481, <https://doi.org/10.1029/1999JB900329>, 2000.
- Vieli, A., Payne, A. J., Shepherd, A., and Du, Z.: Causes of pre-collapse changes of the Larsen B ice shelf: Numerical modelling and assimilation of satellite observations, *Earth and Planetary Science Letters*, 259, 297–306, <https://doi.org/10.1016/j.epsl.2007.04.050>, 2007.
- Weertman, J.: On the sliding of glaciers, *Journal of glaciology*, 3, 33–38, 1957.
- Zoet, L. K. and Iverson, N. R.: A slip law for glaciers on deformable beds, *Science*, 368, 76–78, <https://doi.org/10.1126/SCIENCE.AAZ1183>, 2020.